NTNU
Norwegian University of
Science and Technology

Hybrid membranes to limit amine evaporation in membrane contactors for CO_2 capture

Marta Westad Hauge

Chemical Engineering and Biotechnology
Submission date: June 2017
Supervisor: Liyuan Deng, IKP
Co-supervisor: Luca Ansaloni, IKP
Zhongde Dai, IKP

Norwegian University of Science and Technology
Department of Chemical Engineering

Abstract

In order to meet the global demand of energy from combustion processes with fossil fuels without interfering with the atmospheric levels of CO_2, carbon capture and storage (CCS) is considered a viable solution. Separation of CO_2 from combustion gas performed by absorption/stripping in columns is today a costly and energy demanding process. One way to reduce the energy requirement of CO_2 absorption is to use DEEA MAPA blends, but they are volatile and their use at industrial level is thus problematic.

Membrane based absorption, defined as membrane contactors allow operating with volatile absorbents without emitting harmful chemicals. This require a membrane that allows high CO_2 and low absorbent permeability. Membrane contactors also have the potential to reduce the capital cost of absorption as effective membrane modules increase the surface area of absorption, and thereby reduce the process volume.

This thesis has investigated two different AF2400 membranes with addition of ZIF-8 and XT-RGO nanoparticles, and in particular how these nanocomposite membranes affect characteristics that are important to consider in membrane contactor absorption. The membranes were tested together with a volatile 3rd generation CO_2 absorbent named 3D3M and with MEA as a reference absorbent. It was discovered that the two nanocomposite membranes decreased the permeability of the two amine absorbents substantially compared to the pure AF2400 membrane. However, the nanocomposite membranes also revealed a lower CO_2 permeability compared to pure AF2400. A simple membrane contactor model was proposed to evaluate the membrane module performance in terms of evaporation prevention. Other highly CO_2 permeable membranes were also tested together with 3D3M and two other 3rd generation absorbents - 3DEA2M and 3HEPP2M, where only AF2400 proved to be stable with the absorbents.

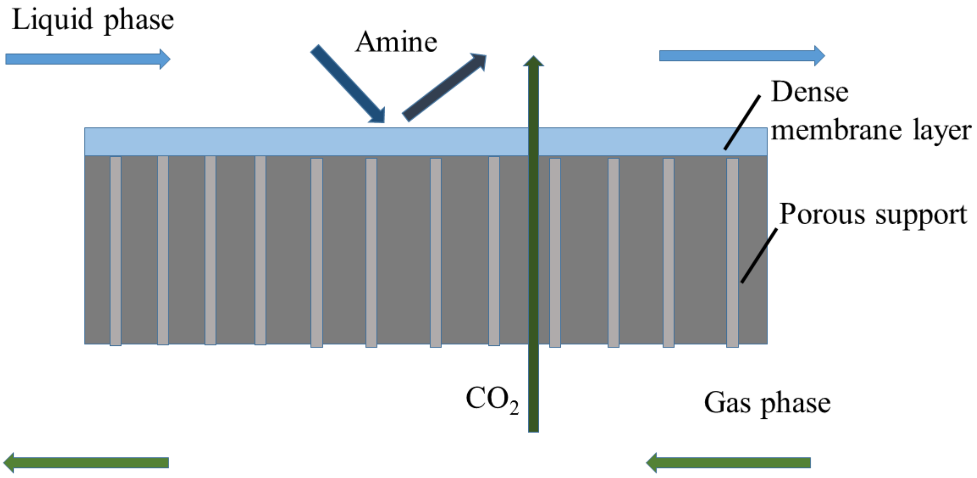

Figure 0.1: Schematic illustration of a membrane contactor.

Sammendrag

Karbonfangst er en teknologi som muliggjør å tilfredsstille det globale energibehovet med forbrenning av fossile brennstoff uten å forstyrre atmosfærenivået av CO_2. I dag blir CO_2 separert fra forbrenningsgasser ved absorpsjon/stripping i kolonner, som er en kostbar og energikrevende prosess. En måte å redusere energikravet til absorpsjon er å benytte seg av en DEEA/MAPA-absorbentmix, men disse er svært volatile aminer som skaper utfordringer ved implementering til industriskala.

Membranbasert absorpsjon, kalt membrankontaktorer, tillater bruk av volatile absorbenter uten hensyn til utslipp. Dette krever at membranen tillater en høy permeabilitet av CO_2 og lav permeabilitet av absorbenter. Membrankontaktorer kan også redusere investeringskostadene til absorpsjon siden effektive membranmoduler øker overflaten mellom gassfase og absorbent, og reduserer dermed prosessvolumet.

Denne masteroppgaven har undersøkt to ulike nanokompsoittmembraner med polymeren AF2400 og nanopartiklene ZIF-8 og XT-RGO for karakteristikker som er viktige i membranabsorpsjon. Membranene ble testet med en volatil CO_2-absorbent kalt 3D3M og med MEA som referanseabsorbent. Det ble konkludert med at begge nanokomposittmembranene senket permeabiliteten til begge absorbentene betraktelig sammenlignet med ren AF2400-membran. Samtidig viste det seg at nanokomposittmembranene senket CO_2-permeabiliteten i forhold til ren AF2400. En enkel membrankontaktormodell ble brukt for å evaluere membranmodulen med tanke på redusering av utslipp. Andre membraner med høy CO_2-permeabilitet ble også testet sammen med 3D3M og to andre 3. generasjonsabsorbenter - 3DEA2M og 3HEPP2M, hvor kun AF2400 viste seg å være kompatibel.

Preface

This Master's Thesis is written spring 2017 at the Norwegian University of Science and Technology, as a part of the Environmental Engineering and Reactor Technology research group. The work has been a part of the 3GMC project delivered by CLIMIT, and supervised by Dr. Liyuan Deng with Dr. Luca Ansaloni and Dr. Zhongde Dai as co-supervisors.

First of all, I would like to thank Liyuan for offering me a thesis I have found interesting and rewarding to work with. I will also like to thank Zhongde for encouragement and fun chats in the lab. Last, but not least I will thank Luca for being available 24/7, answering my stupid and not so stupid questions and helping me out in the lab. I also appreciate all the interesting people I have met in the lab that have helped me or entertained me in spare moments.

Speaking of entertainment, I want to thank my co-students in all floors of chemistry block 4 for making my lunches and cafeteria dinners fun, and offering me a break from my thesis work. I especially want to thank Vilde and Natalie for membrane chats, Eirik for keeping me in company at my desk and Åsmund for making me laugh.

The Bible says you're supposed to honor your mother and father, and in case I might lose my inheritance if I don't, I hereby thank my parents for parenting me. I also have to thank Åsmund's father for proofreading my thesis, and then just not to exclude I have to thank his mother also.

I hereby declare that this is an independent work according to the exam regulations of the Norwegian University of Science and Technology.

Contents

1 Introduction **1**

2 Theory **3**
2.1 Membrane transport 3
2.2 Nanocomposite membranes 5
2.2.1 Polymer phase 6
2.2.2 Nanofillers 7
2.3 Pervaporation 11
2.4 Membrane contactors 13
2.4.1 Mass transfer in membrane contactors 14
2.4.2 CO_2 absorption 15
2.4.3 Absorbent chemicals 16
2.4.4 Hollow fiber coating 17

3 Experimental methods **19**
3.1 Materials 19
3.2 Membrane preparation 19
3.3 Characterization 19
3.3.1 Membrane morphology 19
3.3.2 Membrane compatibility study 19
3.3.3 Amine evaporation 20
3.3.4 Titration 21
3.3.5 Ion chromatography 21
3.3.6 Mixed gas permeation 21
3.3.7 Membrane contactor study 22
3.4 Dip coating of hollow fibers 23

4 Experimental results and discussion **25**
4.1 Nanocomposite membrane morphology 25
4.2 Membrane compatibility study 27
4.3 CO_2 permeability 31
4.4 Amine evaporation 33
4.4.1 CO_2/amine selectivity 34
4.5 Membrane contactor results 36
4.5.1 CO_2/amine selectivity 38
4.6 Dip coating characteristics 39

5 Modelling **43**
5.1 Model theory 43
5.2 Simulation results 45

6 Conclusion **51**

7 Further research **52**

A Titration error **i**

B Membrane preparation **ii**

C Selectivity calculation **iii**

D Morphology of hollow fibers **viii**

E Sensitivity analysis of simple membrane model **ix**

List of Figures

0.1 Schematic illustration of a membrane contactor. i
2.1 Illustration of a membrane separation mechanism. 3
2.2 The Robeson upper bound for CO_2/N_2 separation. 5
2.3 Structural formula of a Teflon AF2400 copolymer 7
2.4 Robeson plot of different AF2400 + nanofiller membranes. 8
2.5 Structural image of a ZIF-8 crystal. 9
2.6 Chemical structure of reduced graphene oxide. 10
2.7 Molecular sieving mechanisms of CO_2 and amine in graphene and ZIF-8. 11
2.8 Illustration of a vacuum pervaporation principle. 12
2.9 Flow scheme of a membrane contactor setup. 13
2.10 Hollow fiber module. 17
3.1 Pervaporation flow sheet 20
3.2 Flow sheet of the mixed gas permeation setup. 22
3.3 Membrane contactor flow sheet. 23
4.1 Cross section S(T)EM images of AF2400/3wt% XT-RGO. 25
4.2 Cross section S(T)EM images of AF2400/3wt% ZIF-8. 26
4.3 Surface S(T)EM image of a AF2400/3wt% ZIF-8 membrane. 26
4.4 Development of weights of membrane pieces in a 3D3M solution. 27
4.5 Development of weights of membrane pieces in a 3DEA2M solution. . . . 28
4.6 Development of weights of membrane pieces in a 3HEPP2M solution. . . 28
4.7 Development of weights of membrane pieces in a MEA solution. 29
4.8 Development of weights of membrane pieces in a H_2O solution. 29
4.9 CO_2 permeabilities of nanocomposite AF2400 membranes. 31
4.10 CO_2/N_2 separation factors of nanocomposite AF2400 membranes. 32
4.11 Prevention of amine emission with addition nanoparticles to AF2400. . . 33
4.12 CO_2/amine selectivity at 50 °C. 35
4.13 CO_2 permeability AF2400/XT-RGO and AF2400/ZIF-8 membrane in membrane contactor. 36
4.14 Difference in CO_2 permeability in MG and MC study for AF2400/XT-RGO membrane. 37
4.15 CO_2/amine selectivity in membrane contactor. 38
4.16 AF2400 thickness layer of big sized polypropylene hollow fibers. 39
4.17 AF2400 thickness layer of medium sized polypropylene hollow fibers. . . . 40

4.18 AF2400 thickness layer of small sized polypropylene hollow fibers. 40
5.1 Effect of Tl and CO_2 permeability on module surface area. 46
5.2 Effect of temperature and α_{CO_2} on η. 47
5.3 Effect of α_{CO_2} and wMEA on η. 48
5.4 Effect of α_{CO_2} and fPp on η. 49
A.1 Titration of a not measurable concentration of MEA in LabX. i
A.2 Titration of a measurable concentration of MEA in LabX. i
B.1 Membrane photos. ii
C.1 Interpolation of CO_2 permeability through AF2400/XT-RGO at 50 °C. . iv
C.2 Interpolation of CO_2 permeability through AF2400/XT-RGO at 50 °C. . iv
C.3 Interpolation of CO_2 permeability through AF2400/ZIF-8 at 50 °C. . . . v
C.4 Interpolation of CO_2 permeability through AF2400/ZIF-8 at 50 °C. . . . v
D.1 Cross section SEM images of tubular fibers coated with AF2400. viii
E.1 Effect of tubular diameter on total surface area and η. ix
E.2 Effect of gas flow on number total surface area and η. ix
E.3 Effect of tube length on total surface area and η. x
E.4 Effect of liquid film layer on total surface area and η. x

List of Tables

2.1 CO_2 permeability and CO_2/N_2 selectivity. 8
4.1 Interpolation table of membrane thickness. 41
5.1 Input parameters to the model. 44
5.2 Output parameters from the model. 45
5.3 Values of input parameters kept constant during sensitivity analysis. . . . 45
5.4 CO_2/amine selectivity of AF2400/ZIF-8 and AF2400/XT-RGO. 47
B.1 Concentration and thickness of the membranes tested in this section. . . ii
C.1 Relative humidity calculation table. iii
C.2 CO_2 permeability at 50°C. vi
C.3 MEA, MAPA and DEEA Antoine parameters. vii
C.4 Saturation pressure of amines. vii
C.5 Final Δp_i values for MEA, MAPA and DEEA. vii

Nomenclature

Symbol	**Unit**	**Description**
P	Barrer	Permeability
D	cm^2/s	Diffusion coefficient
S	cm^3/cm^3cmHg	Solubility coefficient
J_i	mol/sm^2	Flux of component i
c_i	mol/L	Concentration of component i
l	m	Membrane length
α_{ij}	-	Separation factor
y	-	Mol fraction on permeate side
x	-	Mol fraction feed side
T_g	°C	Glass transition temperature
r	1/s	Membrane aging rate
GPU	Barrer/cm	Permeance
Å	10^-10 m	Ångstrøm
σ	N/m	Surface tension
θ		Contact angle
r	m	Pore radius
Ω	-	Weight factor
K		Overall mass transfer coefficient
K_g		Mass transfer coefficient in gas phase
K_m		Membrane mass transfer coefficient
m		Ratio between liquid as gas concentration at equilibrium
E	-	Enhancement factor
K_l	-	Liquid mass transfer coefficient
$K_{m,nw}$		Mass transfer coefficient in non wetted area
$K_{m,w}$		Mass transfer coefficient in wetted area
ξ	-	Liquid loading of absorbent
$\alpha_{\mathrm{CO_2}}$		Membrane CO_2 selectivity
η	-	Prevention of amine evaporation

Symbol	**Description**
CCS	Carbon Capture and Storage
MEA	Monoethanolamine
PTMSP	Poly(1-trimethylsilyl-1-propyne)
PI	Polyimides
AF2400	Amorphous fluorinated polymer
MOF	Metal Organic Framework
ZIF	Zeolitic imidazolate frameworks
XT-RGO	Reduced Graphene Oxide
HEPP	1-(2-Hydroxyethyl)piperidine
MAPA	3-(methylamino)propylamine
DEA	3-(Diethylamino)-1,2-propanediol
DEEA	2-(Diethylamino)ethanol
3HEPP2M	3 molar HEPP + 2 molar MAPA
3DEA2M	3 molar DEA + 2 molar MAPA
3D3M	3 molar DEEA + 3 molar MAPA
FC-72	3M™ Fluorinert™ Liquid

1 Introduction

In a perfect world there should be no combustion of fossil fuels in the energy industry. There are many evidences pointing at fossil fuels as the villain behind poles melting, elevated sea level and loss of species due to changes in climate. Our world as we know it, with all its resources is adjusted to a certain amount of CO_2 in the carbon cycle. By daily producing huge amounts CO_2 from combustion of fossil fuel, we are disturbing our carbon cycle towards a higher equilibrium concentration of CO2 in the atmosphere. Researchers are working hard to find replacements for the use of fossil fuels for energy purposes. We have reached far by for example developing the electric car, biofuels, bioplastics and hydrogen engines, but the development is not running fast enough for us to stop using fossil fuels completely. One way of minimizing the damages on the carbon cycle while we wait for better technology can be to store the CO_2 from the fossil fuels combustion process.

Carbon capture and storage (CCS) is therefore a research field that has gained a lot of attention the past few years. The former Norwegian prime minister Jens Stoltenberg even claimed this research field could be the ”Norwegian moon landing”. The technology is not only useful in an environmental point of view, but is also useful in industry as removal of CO_2 in natural gas raises the heating value of the gas and reduces the gas sourness. The conventional process of separating CO_2 from air is by CO_2 absorption in columns. This is followed by stripping CO_2 off the absorbent in order to recycle the absorbent. Typical chemical absorbents are carbonate buffers and primary, secondary and tertiary alkanolamines, where MEA (monoethanolamine) is the conventional absorbent. This technology make up 90% of the carbon capture market (Zhao et al., 2016) in post-combustion gas treatment, but there are several challenges related to it. According to Rochelle (2009), the power consumption of a MEA absorption process in 2006 was 0.37 MWh/ton CO_2 removed, and the total cost was 52 $/ton CO_2 removed. This is relatively expensive, taking into account that CO_2 removal post combustion is not a mandatory process. One way to reduce the cost is to reduce the energy requirement of the process or reduce the operational cost.

There are other technologies for CO_2 separation from gas on the market today, such as membrane separation and pressure-swing adsorption. These applications face challenges in limitations of compression work, which limits the processes from going below 0.21 MWh/ton CO_2 (Rochelle, 2009).

Membrane contactors offer a technology at the interface between classic membrane separation and conventional CO_2 absorption. CO_2 is still separated from a gas stream by a membrane, but instead of going directly to gas phase, there is a liquid on the other side of the membrane with a selective absorbent that binds to CO_2. In the same way as for conventional absorption the absorbent and CO_2 will be separated in order to release the ”captured” CO_2 and regenerate the absorbent in a stripper component of the process. This will also be performed in a membrane contactor unit.

According to Zhao et al. (2016) membrane contactors have the potential to reduce both capital and operating cost by 30 - 40 % compared to traditional processes. This is due to the fact that membrane contactors consist of efficient modules that increase the specific surface area between gas stream and absorbent liquid, and hence the required volume of the process.

Since the membrane in membrane contactors provide a selective interface between absorbent liquid and gas phase, membrane contactors can in addition to reducing capital and operating cost offer a reduction in emission of absorbent liquids compared to conventional absorption. In conventional absorption the absorbent can evaporate in the absorption column and be released together with the gas cleaned from CO_2, and in order to prevent this, an additional process unit - amine scrubber has to be added. Economically and environmentally it is desirable to reduce the loss of absorbents.

In the last years, few 3rd generation CO_2 absorbents have been mentioned in literature that require less energy to be separated from CO_2 in the stripper process, and hence lowering the energy requirement of CO_2 separation. Unfortunately, many of these 3rd generation absorbents are quite volatile and harmful to human health and environment. This is an unfortunate combination in conventional gas absorption, where higher volatility of absorbents is equivalent to higher emissions of absorbents. The aim in membrane contactors is to make membranes that can withold even volatile absorbents, such that volatility is not a concern for absorbents with favourable CO_2 absorption characteristics.

The aim of this Master's Thesis is to find a membrane that satisfyingly performs when in contact with a 3rd generation absorbent, such that the membrane does not dissolve or absorb the absorbent. It will also be studied if modifying the membrane by adding nanoparticles will contribute to a decrease in the emission of amines without reducing the flux of CO_2 through the membrane. In addition, synthesis of effective membrane modules will be investigated. Finally, a simple membrane contactor model will be simulated in MATLAB in order to find which process parameters that are sensitive in relation to amine emission.

2 Theory

Membranes are selective barriers that allow some species to penetrate its barrier while it prevents others. The mechanism is shown in Figure 2.1. The part of the feed flow that penetrates the membrane is called permeate, and the part that is rejected is called retentate. The speed of the permeation is decided by a driving force across the membrane, depending on the chemical potential which is related to differences in pressure, concentration or electrical potential. Membranes occur naturally in living cells, where they control what is allowed to enter and leave the cell. In the previous century the potential of artificial tailored membranes to act as separators was discovered. The first membrane for gas separation in industrial applications was made in 1980 by Permea (Baker, 2002), and in 2002 , membrane gas separation was reported to be a $150 million/year industry.

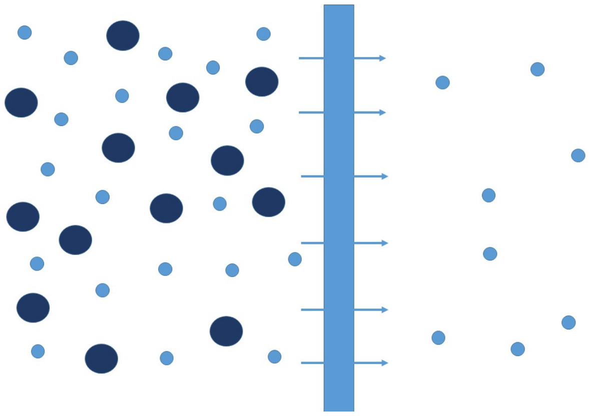

Figure 2.1: Illustration of a membrane separation mechanism. The blue line is the membrane barrier, and the particles on the right side is the permeate.

2.1 Membrane transport

In principle, there are four ways to permeate through a membrane, and the type of permeation depends on the pore sizes of the membrane. If a penetrant permeates through a pore of size 0.1 to 10 μm it permeates by convective flow, while if the pore is smaller than 0.1 μm it permeates according to Knudsen diffusion. If the pore size is between 5 - 20 Å, permeation is characterized as molecular sieving. If the membrane is dense permeation occurs via solution diffusion. Pore sizes between 5 and 10 Å are regarded as being in the transition range between microporous membranes with molecular sieving mechanisms and dense membranes with solution diffusion. In commercial use of membranes for gas separation, dense polymeric layers characterized by solution diffusion mechanism are the most commonly used type of membrane.

Permeability, P, is a measure of the flow rate of a species through a membrane when pressure is the driving force. Permeability is a value independent of membrane thickness, meaning that it is the same for same membranes at with different thickness values. P

[Barrer] in dense membranes by solution diffusion is defined by Equation 2.1:

$$P = D \cdot S \tag{2.1}$$

Where D is the diffusion coefficient $[cm^2/s]$, a kinetic parameter that depends on the size and geometry of the permeating compound. S is the solubility coefficient $[cm^3/cm^3$ cmHg], a thermodynamic parameter which describes the degree of penetrants being sorbed by the membrane at equilibrium conditions.

Flux,J is another measure of flow through a membrane, which is opposite to permeability not independent of thickness. J $[mol/sm^2]$ for a component i through a membrane is described by Fick's law:

$$J_i = -D_i \frac{dc_i}{dx} \tag{2.2}$$

Where dc_i is the concentration difference over a length x for a component i, while the differential dc_i/dx expresses the concentration gradient over the membrane. In gaseous systems the concentration difference is expressed as partial pressure difference across the membrane, Δp_i. Solving Equation 2.2 for the boundary conditions that applies in case of gas permeation, it is possible to obtain the permeance $[Barrer/cm]$ of a penetrant through a membrane with thickness l [m]:

$$\frac{P_i}{l} = \frac{J_i}{\Delta p_i} \tag{2.3}$$

Another relevant term in gas separation is the separation factor of component i compared to a component j, α_{ij}:

$$\alpha_{ij} = \frac{y_i/y_j}{x_i/x_j} \tag{2.4}$$

Where y is the mole fraction in the permeate side, and x is the mole fraction in the feed side.

Separation factor and permeability are regarded as trade-off parameters in polymer membranes. An increase in separation factor will often lead to a lower permeability, and conversely. The ideal case is to achieve a high membrane separation factor and high permeability of the desired permeate. Robeson plot is a method to compare membrane performance in terms of permeability (P) and selectivity ($\alpha_{\mathrm{CO_2}}$).

The Robeson plot for CO_2 and N_2 is given in Figure 2.2, where the black line represents the upper performance of separation of CO_2 and N_2 by polymer membranes reported in 2008 (Robeson, 2008). This line is also called the Robeson upper bound. According to Chung et al. (2007) inorganic membranes can lie far above the upper bound. Combining polymer membranes with addition of inorganic fillers is one way to increase permeability and the separation factor. In order to keep polymer membranes dense, combination of polymer and inorganic membranes can be done by dispersing an inorganic filler at nanoscale in the polymer. This type of membrane is called nanocomposite membrane.

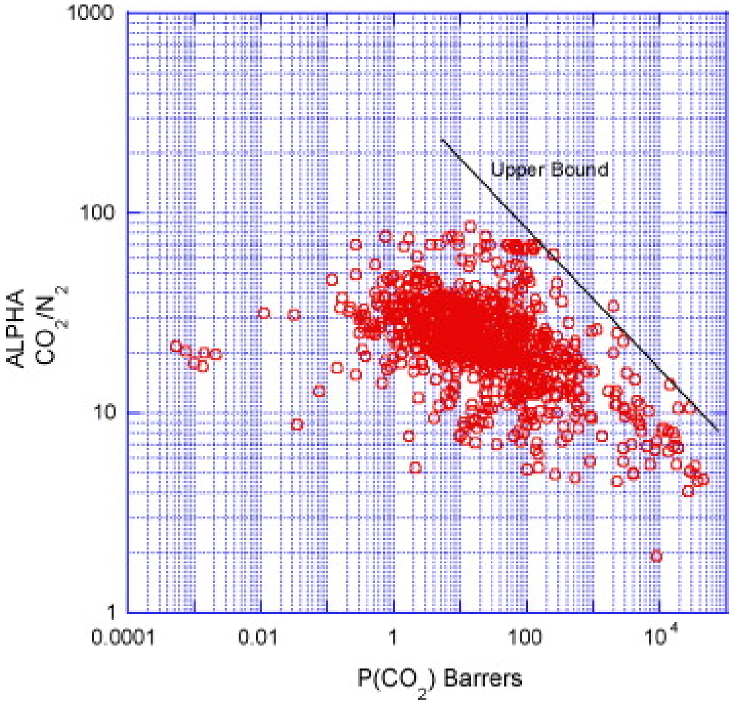

Figure 2.2: The Robeson upper bound for CO_2/N_2 separation represented by the black line. The red dots are experimental values of CO_2 permeability against CO_2/N_2 selectivity (Robeson, 2008).

2.2 Nanocomposite membranes

Nanocomposite membranes are membranes where dispersed inorganic particles are embedded in a polymer matrix at nanometer scale. This type of membranes combines the positive characteristics of both polymer and inorganic membranes. According to Koros (2002), polymer membranes provide a high flexibility and processability, which makes them easier to apply in more effective spiral-wound or hollow fiber modules. On the other hand, this flexibility makes it difficult for the membrane to act selectively on molecules of similar size, and polymer membranes also suffer from performance loss with time. Inorganic membranes are more thermally stable than polymers and they also provide molecular sieving mechanisms which can discriminate molecules of similar size. However, inorganic membranes are more expensive and their brittleness make them hard to scale up (Pandey and Chauhan, 2001).

The combination of polymers and inorganic compounds in membranes can provide useful characteristics in gas separation. Cong et al. (2007) reports that organic functional groups in the polymer can help disperse the inorganic compounds better. Also, the combination of functional groups on inorganic surfaces may improve transport and absorption properties which can lead to improved permeability and selectivity. In order to achieve a reliable measurement of the membrane performance, it is important to obtain a homogeneous membrane with well dispersed nanoparticles. The overall goal of adding nanoparticles in membranes for use in membrane contactors is to reduce the amine flux through the membrane without affecting the CO_2 flux compared to pure polymer membranes.

The affinity between the nanoparticle and polymer matrix is an important factor in nanocomposite membrane morphology. Ideally, the nanoparticles fills the polymer matrix perfectly, and no holes surround the nanoparticle. In case of voids between the nanoparticle and polymer phase, the formation is called sieve-in-cage or leaky interface. This type of hole increases the permeability of the membrane. If in addition the nanoparticles agglomerate, and there are voids surrounding the nanoparticle cluster, the selectivity will decrease. Another possible unfavourable morphology is a rigidified polymer phase surrounding the nanoparticle. This type of structure will decrease the permeability but increase the selectivity of the membrane. It is also possible that a pore surrounding the nanoparticle is completely blocked for penetration. This type of affinity will only decrease the permeability and have no positive effect on the selectivity (Ansaloni, 2016).

2.2.1 Polymer phase

High free volume glassy polymers possess high gas permeabilities. Among high free volume glassy polymers commercially available are poly(norbornene), polyacetylenes (eg: PTMSP), perfluoropolymers (eg: Teflon AF2400), polymers of intrinsic microporosity (PIM) and polyimide (PI). High fractional free volumes lead to high permeabilities (Budd and McKeown, 2010). In this thesis, AF2400 is the main membrane studied, mainly based on the fact that AF2400 has a low permeability in case of organic vapors, which is promising for membrane contactor setups where prevention of amine evaporation is desirable. (Nemser and Roman, 1991) (Ansaloni et al., 2016)

AF2400 is a perfluorinated copolymer with 87 mol% 2,2-bistrifluoromethyl-4,5-difluoro-1,3-dioxole and 13 mol% tetrafluoroethylene, with structural formula shown in Figure 2.3. It is classified as an amorphous and glassy polymer with a high free fractional volume of 0.327. The glass transition temperature (T_G) of AF2400 is 240 °C (Lowry et al., 1992), which is the background for the epithet 2400, and the polymer starts to decompose above 360 °C (FC, 2016).

Teflon AF2400 also has a high CO_2 permeability, according to Nguyen et al. (2011) approximately 3900 barrers. This permeability is lower compared to polymers such as PTMSP but in return, according to Tokarev et al. (2006) the polymer is known to be more chemically stable and has a lower swelling and aging tendency than PTMSP. The aging rate, r for AF2400 is $1.0r \cdot 10^3$ while it is $6.3r \cdot 10^3$ for PTMSP (Tiwari et al., 2015).

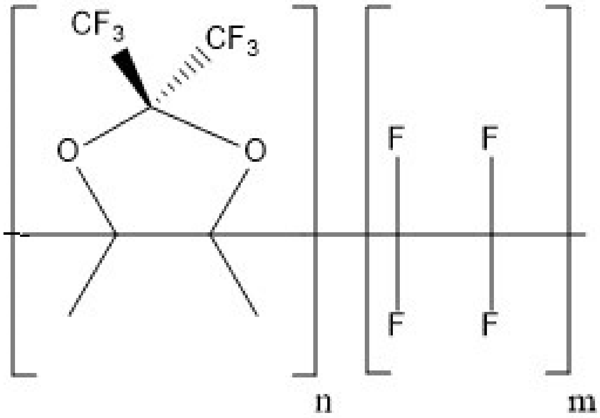

Figure 2.3: Structural formula of a Teflon AF2400 copolymer. n indicate the number of monomers in the left bracket, while m indicate the number of monomers in the right bracket (Pinnau and Toy, 1996).

2.2.2 Nanofillers

Nanofillers are particles that have at least one dimension in nano scale range that can be used as a filler in a polymer matrix. There are several promising nanofillers reported in literature, such as: metal organic frameworks (MOF's), porous aromatic framework (PAF), carbon nanotubes, zeolites and graphene (Ansaloni, 2016). In a previous project, two different types of graphene and MOF immersed AF2400 membranes were tested for CO_2 permeability and CO_2/N_2 selectivity in a gas permeation setup. Figure 2.4 shows the Robeson plot with the results from this particular study. Here it is evident that neither pure AF2400 or AF2400 mixed matrix membranes perform anywhere near the Robeson 2008 upper bound. According to Low et al. (2013) the permeance of CO_2 should be more than 1000 GPU and the CO_2/N_2 selectivity should be between 20-100 in order to be attractive in post-combustion processes. In Table 2.1 the results from the Robeson plot is shown in numbers, and it can be seen that none of the membranes perform near the selectivity demanded for gas separation membranes. Yet, this does not exclude AF2400 membranes for being used in membrane contactor separation of CO_2. AF2400 is as mentioned a chemical stable polymer and has low permeability for organic compounds. In addition, the CO_2/N_2 separation factor is not a very important factor in membrane contactors, where CO_2 permeability and CO_2/absorbent selectivity are more important.

Table 2.1: CO_2 permeability and CO_2/N_2 α for different AF2400 nanocomposite membranes tested at room temperature and 0% relative humidity.

Membrane	CO_2 perm. [Barrer]	α
AF2400	4800	4.1
AF2400 + 1 wt% XT-RGO	4200	3.9
AF2400 + 1 wt% XT-15	4100	3.1
AF2400 + 3 wt% ZIF-L	4500	3.2
AF2400 + 7 wt% ZIF-L	3500	4.2
AF2400 + 3 wt% ZIF-8	4500	4.1
AF2400 + 7 wt% ZIF-8	4600	3.9

Based on the data in Table 2.1 it was decided to study only ZIF-8 and XT-RGO further. In reality, many of the nanoparticle immersed membranes did not perform significantly differently, but because of more time consuming upcoming analyzes ZIF-8 and XT-RGO were chosen based on a slightly better performance than the other nanoparticles. None of the nanoparticles proved to increase CO_2 permeability, and the selectivity was either approximately the same as for AF2400 or lower, except for 7wt% ZIF-L, which also had the lowest CO_2 permeability. As mentioned, the most important factor in membrane contactors is the selectivity between CO_2 and absorbents, so these results do not contradict adding nanoparticles to AF2400 for membrane contactor applications.

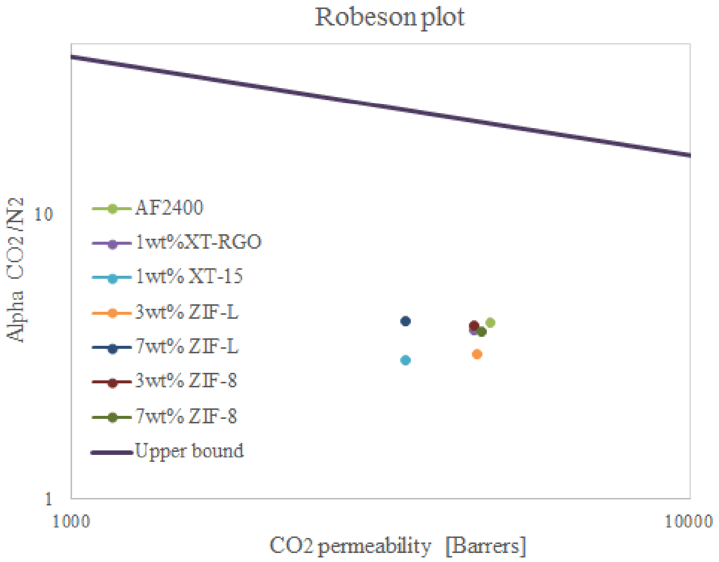

Figure 2.4: Robeson plot of different AF2400 + nanofiller membranes plotted together with the Robeson upper bound for CO_2 and N_2 separation per 2008 (Hauge, 2016).

Zeolitic imidazolate frameworks (ZIF) is an umbrella term for highly ordered porous solids consisting of zink ions bridged by imidazolate ligands in a tetrahedal geometry. According to Low et al. (2014) the organic compounds in ZIF contribute to the nanoparticles filling the polymer better, which improves the phase inversion process. ZIFs are also reported by D'Alessandro et al. (2010) to have high adsorption rate of CO_2, in addition to being hydrophobic and thermally and chemically stable. The type of ZIF studied in this project is ZIF-8 which structure can be seen in Figure 2.5.

ZIF-8 is reported by Zhang et al. (2013) to have a pore with a kinetic size of 3.4 Å. Yet, the structure is flexible, as penetrants of kinetic diameter 4.30 to 5.85 Å have been reported to permeate through the crystal. In comparison, CO_2 and N_2 have kinetic sizes of 3.30 and 3.64 Å, respectively (Thallapally et al., 2008).

ZIF-8 is has a permeability of CO_2 of 2800 Barrer and a CO_2/N_2 selectivity of 2.8 at 25 °C and 1 bar feed pressure (McCarthy et al., 2010). This is both a lower permeability and selectivity compared to pure AF2400 membranes. The goal is that the polymer + nanoparticle membrane matrix will obtain characteristics that increase the separation factor of the membrane, by ZIF-8 acting as a molecular sieve in the polymer matrix.

ZIF-8 is reported by Liu et al. (2017) to be of low cost, simple to manufacture and being simple to prepare. It also has the potential of forming water channels, due to small hydrophobic areas inside the crystal that forces water to permeate quickly.

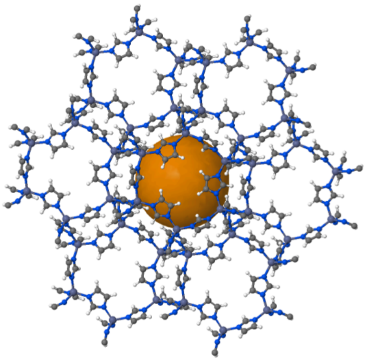

Figure 2.5: Structural image of a ZIF-8 crystal. The orange area indicate the pore area where gas molecules can penetrate. (Greeves, 2016)

Graphene is known for its chemical inertness, mechanical endurance and thermal stability. Graphene has a melting temperature of 4237 °C, which makes it compatible with industrial temperatures (Los et al., 2015). It consists of a single layer of carbon atoms, which electrical configuration makes pure graphene impermeable for even small molecules such as helium. Yet, it is possible to make artificial holes to the graphene layer, and based on the hole size make it possible to decide a molecular size exclusion. Else, graphene layers will act as a layered molecular sieving structure (Huang et al., 2015).

The graphene material studied in this thesis is reduced graphene oxide (XT-RGO), which chemical structure is displayed in Figure 2.6. It is derived from graphene oxide, where the oxygen containing groups are reduced. If more oxygen atoms are removed from graphene oxide, reduced graphene oxide is more similar to pure graphene (Osilla, 2017). Normally, reduced graphene oxide contains between 77-87 % carbon and 13-22 % oxygen (AZOnano, 2017).

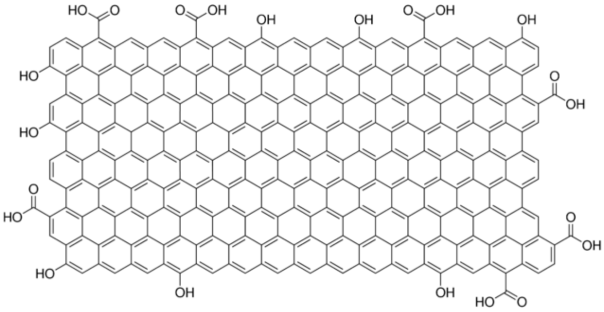

Figure 2.6: Chemical structure of reduced graphene oxide. (Sigma-Aldrich, 2017)

The aim is that graphene and ZIF-8 will disperse in the membrane matrix. Graphene will make impermeable layers which will make small molecules such as CO_2 permeate faster than other compounds between the layers. ZIF-8 has specific a hole that is permeable for CO_2 which will make CO_2 permeate faster through the membrane, and thereby make detours for larger compounds, such as CO_2 absorbents. The procedures are illustrated in Figure 2.7:

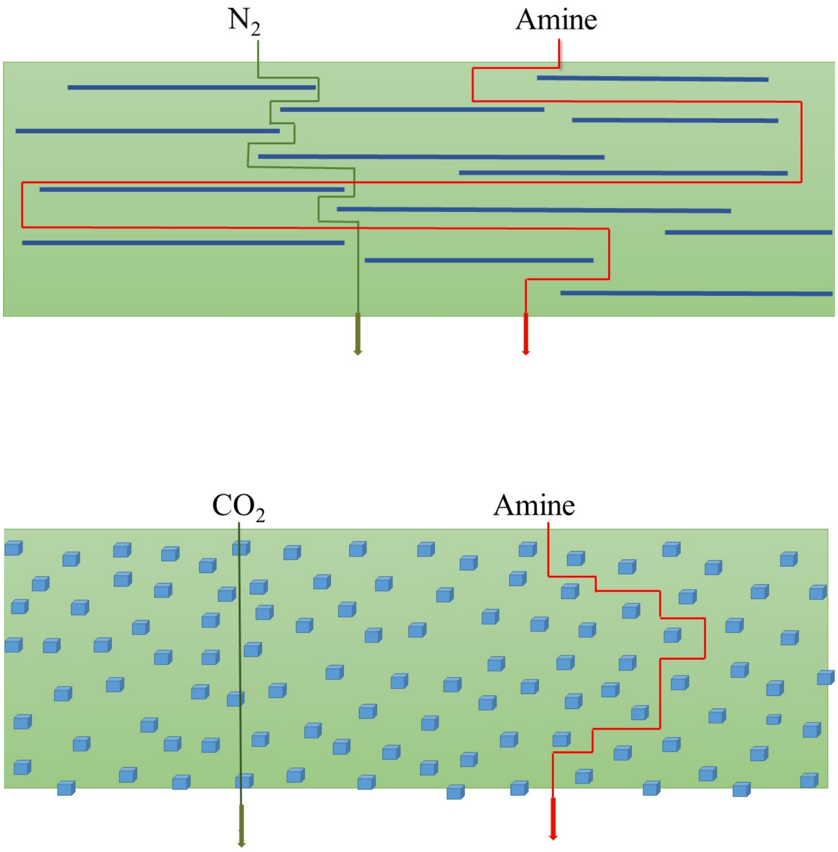

[a]

[b]

Figure 2.7: Molecular sieving mechanisms of CO_2 and amine in [a]: graphene, indicated by blue lines and [b]: ZIF-8 indicated by blue cubes. The green area is the AF2400 polymer matrix.

2.3 Pervaporation

Pervaporation is a membrane separation technique where the membrane separates two liquids from each other. The feed is in contact with one side of the membrane and the product is permeated through the membrane as a low pressure vapor. The product can either be condensed in order to be collected or released.

The driving force in a pervaporation setup is the chemical potential gradient across the membrane, and this can be created by pulling vacuum on the permeate side in order to maintain a lower pressure on the permeate side compared to the feed side, as chemical potential of a compound can be approximated as its partial pressure. This type of pervaporation is called vacuum pervaporation, and is illustrated in Figure 2.8.

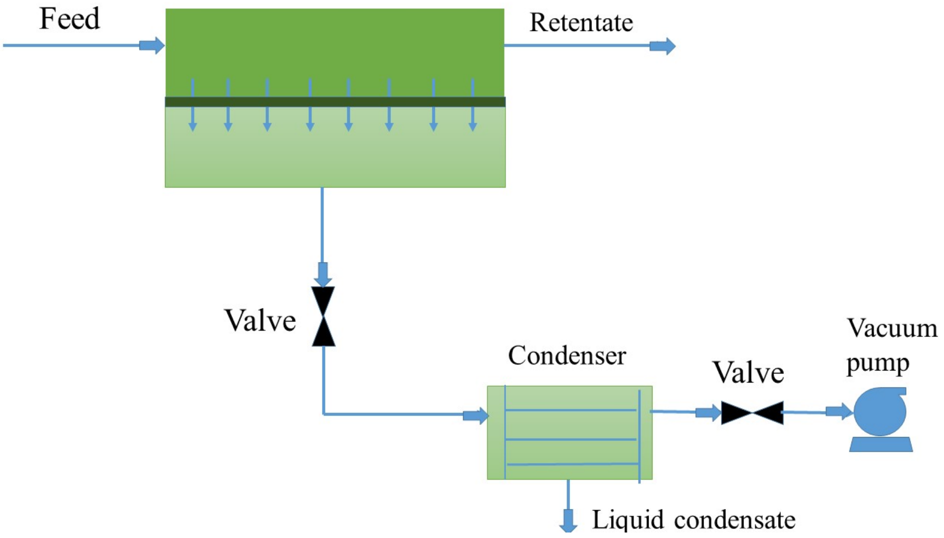

Figure 2.8: Illustration of a vacuum pervaporation principle. The dark green area indicate the membrane. The black triangles are valves.

Pervaporation is according to Feng and Huang (1997) classified into three different applications: dehydration of organic solvents, removal of organic compounds from aqueous solutions, and separation of anhydrous organic mixtures. In this context, pervaporation is used in order to study removal of organic compounds from aqueous solutions. Specifically, the removal of amines from aqueous solutions, in order to study the potential amine emission from a membrane contactor. According to Nguyen et al. (2010) the activity coefficient of amines are reduced when bound to CO_2, and hence the amine volatility will decrease, meaning the actual amine emission will be lower in a membrane contactor system for absorption compared to an amine pervaporation system.

2.4 Membrane contactors

A membrane contactor is an apparatus which offers mass transfer between a gas and a liquid without dispersion of the two phases. This is achieved by allowing fluids to flow on opposite sides of a membrane. This technique can be utilized in absorption processes, as several challenges compared to the conventional absorption technology are diminished, such as flooding at high flow rates, unloading at high flow rates, formation of emulsions and required density difference between fluids (Gabelman and Hwang, 1999). The technique can be used both to absorb and desorb gases, as suggested in Figure 2.9.

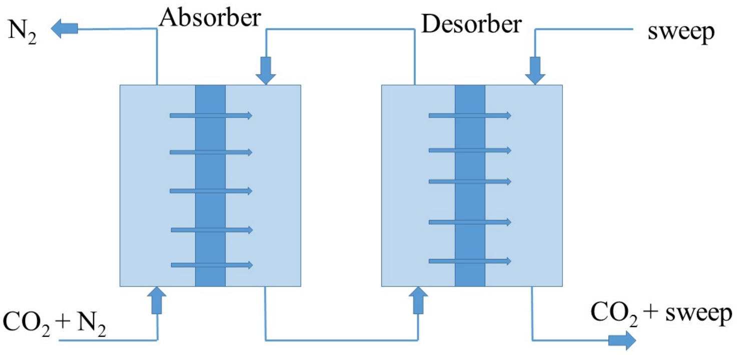

Figure 2.9: Flow scheme of a membrane contactor setup. The dark blue area indicate the membrane. An absorbent is also present in the process, but is recycled.

Membrane contactors offer a much higher specific area compared to conventional gas absorption, allowing a more compact process. Whereas absorption towers have specific areas between 100-250 m^2/m^3, membrane contactors can have more than 1000 m^2/m^3. This is due to the fact that membrane contactors can have effective modules such as hollow fiber or spiral wound. This contributes to a more efficient absorption, as the contact area between CO_2 and absorbent is higher (Deng, 2016a).

Membrane contactors are also prone to challenges. The main challenges are according to Deng (2016a) formation of wetting or bubbling on the membrane surface and evaporation of solvent. The chemical compatibility between solvent and membrane is therefore a main concern when choosing membrane material and absorption chemical. In addition, permeability of absorbent through the membrane and membrane stability are important factors to consider.

Wetting is a consequence of interactions between membrane material and solvent. Ideally, the membrane pores should be filled with fluids from the gas side, but if the fluid on the liquid side is wetting the membrane surface, there is a risk of liquid penetration into the membrane pores. The consequence from liquid pore penetration is an increased mass transfer resistance. The minimum pressure to be applied on the liquid absorbent in order to penetrate membrane pores is called breakthrough pressure, and is given by Equation

2.5 (Li and Chen, 2005).

$$\Delta P = \frac{2\sigma cos\Theta}{r} \tag{2.5}$$

Where σ [N/m] is the liquid surface tension, Θ is the contact angle between the liquid and the membrane, and r is the maximum pore radius. This implies that membranes with smaller pores and/or higher contact angles increase the breakthrough pressure. The absorbent chemicals that are used in the membrane contactor are water soluble, and thus are dense, hydrophobic membrane materials more suitable in order to reduce wetting. However, increasing the amine concentration of absorbent chemical reduces the liquid surface tension (σ), which leads to a reduced breakthrough pressure. This limits the concentration of amines allowed in solution in membrane contactors.

Evaporation of solvent is both an economical and ecological concern. Since the absorption chemical is recycled in the process, it is more economical if the loss of chemical is kept at a low level. The absorbents studied in this thesis are ethanolamines, which are hazardous to living organisms. According to Mertens et al. (2013) these compounds degrade to NH_3 in air which is regarded a pollutant. Emissions of NH_3 cause euthrophication of soil and acid deposition, which affects the quality of water and soil. NH_3 can also cause aerosols in air, which is directly harmful to humans (Adams, 2010).

Another important economical concern is membrane stability. This both concerns the thermal and chemical stability of the membrane. Thermal stability means in this context that the membrane does not degrade or suffer large changes in morphology, while chemical stability means that the membrane does not react chemically with the absorbent. One important thing to check before applying a membrane and an absorbent in a membrane contactor system is therefore the membrane compatibility between the absorption solvent and the membrane material. It is not desirable that the membrane dissolves in the solvent nor that it absorbs the absorbent to a significant extent. The chemical compatibility can be studied by dipping polymer samples in the solvent and observe the dissolution or monitoring the weight factor Ω shown in Equation 2.6:

$$\Omega = \frac{\text{Measured weight}}{\text{Initial weight}} \tag{2.6}$$

2.4.1 Mass transfer in membrane contactors

Mass transfer in membrane absorption systems is described by resistances in series. Resistance in a gas filled pore is described by Equation 2.7:

$$\frac{1}{K} = \frac{1}{K_g} + \frac{1}{K_m} + \frac{1}{mEk_l} \tag{2.7}$$

Here, K is overall mass transfer resistance coefficient, K_g is mass transfer coefficient in gas, K_m is mass transfer coefficient in membrane and K_l is the mass transfer coefficient in liquid. m is the ratio between liquid and gas concentration at equilibrium and E is an enhancement factor due to chemical reaction (Franco et al., 2011). If the membrane contactor contains a membrane module with thin composite membrane layer and porous support, the overall mass transfer resistance coefficient is expressed as in Equation 2.8

$$\frac{1}{K} = \frac{1}{K_g} + \frac{1}{K_{m,t}} + \frac{1}{K_{m,p}} \frac{1}{mEk_l} \tag{2.8}$$

Where $K_{m,t}$ is the mass transfer coefficient in the thin composite layer and $k_{m,p}$ is the mass transfer coefficient in the porous support.

2.4.2 CO_2 absorption

Sorption is a process where one substance is attached to another. Absorption is one type of sorption where the substances get attached in the bulk phase of a gas, liquid or solid. According to Aaron and Tsouris (2005) CO_2 absorption relies on the absorbents affinity with CO_2 to dissolve CO_2 and not other compounds in the gas stream to be purified from CO_2.

Absorbents can either have a physical or a chemical character. The focus of this thesis is on chemical absorbents, specifically alkanolamines. Alkanolamines are organic compounds with an alkane backbone with both hydroxyl and amino groups attached. Alkanolamines can be primary, secondary or tertiary depending on how many carbon atoms the nitrogen atom in the amine group is attached to. In equations 2.9 - 2.14 the absorption reactions between primary, secondary and tertiary alkanolamines and CO_2 are given (Knuutila and Svendsen, 2016):

$$2\,H_2O{=}H_3O^+ + OH^- \tag{2.9}$$

$$CO_2 + 2\,H_2O = HCO_3{}^- + H_3O^+ \tag{2.10}$$

$$RNH_2 + H^+ = RNH_3{}^+ \tag{2.11}$$

Carbamate formation (primary alkanolamine):

$$RNH_2{}^+COO^- + B = RNHCOO^- + BH^+ \tag{2.12}$$

Carbamate formation (secondary alkanolamine):

$$2\,RNH_2 + CO_2 = RNHCOO^- + RNH_3{}^+ \tag{2.13}$$

Total reaction for tertiary alkanolamine:

$$CO_2 + H_2O + R_3N = HCO_3{}^- + R_3NH^+ \tag{2.14}$$

2.4.3 Absorbent chemicals

MEA (monoethanolamine) is an often used absorbent and is in this thesis used as a reference absorbent. According to Kittel et al. (2009) it is the most corrosive of all amines when compared to secondary or tertiary amines. It is therefore desirable to find other alkanolamines for industrial applications.

Combining two different alkanolamines has proven to be effective, and makes it possible to combine desired characteristics. Examples of promising 3rd generation hybrid mixtures of alkanolamines are 3D3M, 3HEPP2M and 3DEA2M. Both are under development at the Environmental Engineering and Reactor Technology research group NTNU, and are proved to be promising in terms of regeneration energy requirement. 3HEPP2M is an abbreviation of 3M 1-(2-Hydroxyethyl)piperidine (HEPP) and 2M 3-(methylamino)propylamine (MAPA), and 3DEA2M is an abbreviation of 3M 3-(Diethylamino)-1,2-propanediol (DEA) and 2M MAPA.

3D3M is the solvent studied primarily in this thesis. 3D3M is an abbreviation for 3M 2-(Diethylamino)ethanol (DEEA) and 3M MAPA. According to Ciftja et al. (2013) this combination of solvents offer a high equilibrium temperature sensitivity, high CO_2 loading and low energy requirement to regenerate the absorbent. Based on numbers from Sigma-Aldrich the boiling point of MAPA and DEEA is lower compared to MEA, making 3D3M a more volatile compound in comparison with MEA.

MAPA is a diamine and contains one primary and one secondary amine group. This structure leads to a high reaction rate and a high absorption capacity. However, the stripping heat of reaction for MAPA is high, meaning that it is difficult to strip off CO_2 from MAPA. DEEA on the other side is a tertiary alkanolamine which has a similar chemical structure to MEA, where two hydrogen atoms on the nitrogen atom in MEA are substituted with two ethyl groups. It is possible to manufacture DEEA from renewable sources such as agricultural products or residues. Opposite to MAPA, the reactivity with CO_2 is low, but primary or secondary amines can act as activators in order to increase the absorption rate of DEEA (Kim and Svendsen, 2007). Combining MAPA with DEEA in solution will therefore enhance the absorption rate of DEEA. In addition this combination of alkanolamines has a potential to decrease the energy requirement of the desorber/stripper part of the process. This is due to the fact that the two chemicals form two liquid phases after absorption, where one phase has a higher loading of CO_2. This makes it possible to separate the absorbents after absorption of CO_2 and only send parts of the liquid to the desorber/stripper which reduces the energy needed to reach the process conditions of desorbing (Ciftja et al., 2013).

2.4.4 Hollow fiber coating

The experiments performed in this thesis are based on self standing flat sheet membranes. In real applications, an efficient membrane module would be used in order to increase the specific mass transfer area per volume (packing density) using a thinner membrane and thus a lower mass transfer resistance. Hollow fiber membrane modules are the modules most referred to in literature. In hollow fiber modules the membrane consist of a thin layer coated on a porous tubular fibers bundled together in a pressure vessel. The feed flow can either enter through the tubular material or outside the tubular material, letting the tubular material collect the permeate. .

Hollow fiber modules have a high packing density. According to Deng (2016b), hollow fibers can have up to 30000 m^2/m^3 in packing density. In Figure 2.10 an example of a hollow fiber module patent is shown, and it can be seen that the module is quite compact.

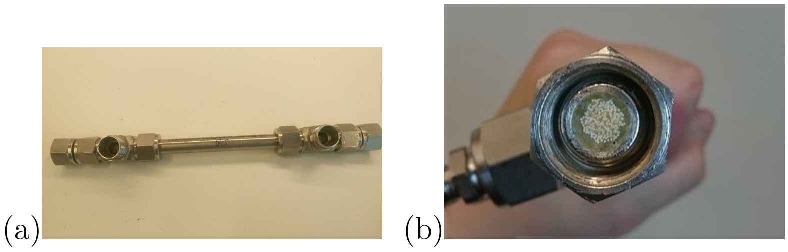

Figure 2.10: (a) Hollow fiber module. (b) Cross-section of hollow fiber module.

3 Experimental methods

3.1 Materials

Basolite Z1200 (ZIF-8) was ordered from Sigma Aldrich and Graphene XT-RGO was delivered by project GNext. Electronic liquid FC-72 was purchased from 3M Belgium and Teflon AF 2400 was purchased from DuPont. CO_2 Bioinert 10% with 90% N_2 and compressed methane (CH_4) were delivered by AGA. The etanolamines MEA (monoethanolamine), MAPA (3-(methylamino)propylamine), DEEA (2-(Diethylamino)ethanol), DEA (3-(Diethylamino)-1,2-propanediol) and HEPP (1-(2-Hydroxyethyl)piperidine) were purchased from Sigma Aldrich.

3.2 Membrane preparation

The mixed matrix membranes were prepared by a solution of 1wt% AF2400 in a FC-72 solution. The nanoparticles (XT-RGO and ZIF-8) were added to the solution corresponding to 3 wt% of the weight of AF2400. The solution was stirred over night, and later exposed to sonication (VWR ultrasonic cleaner). The AF2400/ZIF-8 mix was sonicated for 2 x 45 minutes while the AF2400/XT-RGO mix was sonicated for 8 x 40 minutes. Immediately after sonication, the membrane solution was casted in a Petri dish and dried in a fumehood with a lid covering the Petri dish in order to obtain a controlled evaporation. After drying, the membrane was detached from the Petri dish by using a tweezer. The membranes were then dried in a vacuum oven at 200°C for 24 hours. The membrane thickness was found from an average of 25 measurements in a digital micrometer (Mitutoyo corporation, US). The membrane thicknesses and nanoparticle concentrations of the membranes used in this thesis are given in Appendix B.

3.3 Characterization

3.3.1 Membrane morphology

The membrane morphology of the AF2400/XT-RGO and AF2400/ZIF-8 membranes was studied in a Scanning Electron Microscopy (SEM), S-5500 S(T)EM (Hitachi). Before the membrane sample was inserted to the machine, it was coated with 5 nm of a (20/80) mix of Palladium and Platinum with a sputter coater. The membrane surface samples were cut with a knife, while the cross-sectional samples were torn while dipped in liquid nitrogen in order to obtain a smooth cut.

3.3.2 Membrane compatibility study

In order to investigate different polymer membranes or different CO_2 absorbents in the membrane contactor setup, the compatibility between four different polymer membranes and four different CO_2 absorbents was investigated in addition to water. The polymer membranes investigated were AF2400, PTMSP, PIM-1 and 6FDA-durene. The CO_2 absorbents investigated were 3D3M, MEA, 3DEA2M and 3HEPP2M. Two easily distinguishable geometric shapes were cut out from each membrane, weighed, and placed in a closed container with a CO_2 absorbent and stored at 50°C. The membrane samples were then paper dried, weighed and reimmersed into the absorbent after 1, 3, 7, 24, 48, 120, 312, 864 and 984 hours. All weights were divided by the initial weight, and an average of change in weight was calculated based on the two membrane pieces.

3.3.3 Amine evaporation

In order to study the amine evaporation through the membrane, the membrane was studied in a membrane pervaporation setup with the CO_2 absorbent, shown in Figure 3.1. The particular fluid studied was recirculated in the system at 0.2 mL/min, and vacuum was pulled from the downstream side of the membrane so the pressure was approximately 3 mBar. The permeate was collected in a cold trap that was weighed before and after each trial. A sample was collected from the feed before and after each trial, in addition to one sample from the permeate in order to find the liquid concentration. This was performed on both water, 5M MEA and 3D3M for AF2400 + XT-RGO and AF2400 + ZIF-8. In the MEA trials, the concentration of the samples was found by titration, while for 3D3M the concentration was found by ion chromatography since titration only detects concentration of amines in general and not specific compounds. The test was only run at 50°C, since the experiment was very time consuming. Each test had to run for 8 - 10 hours in order to collect enough permeate, and was performed 3 times in order to get an average value.

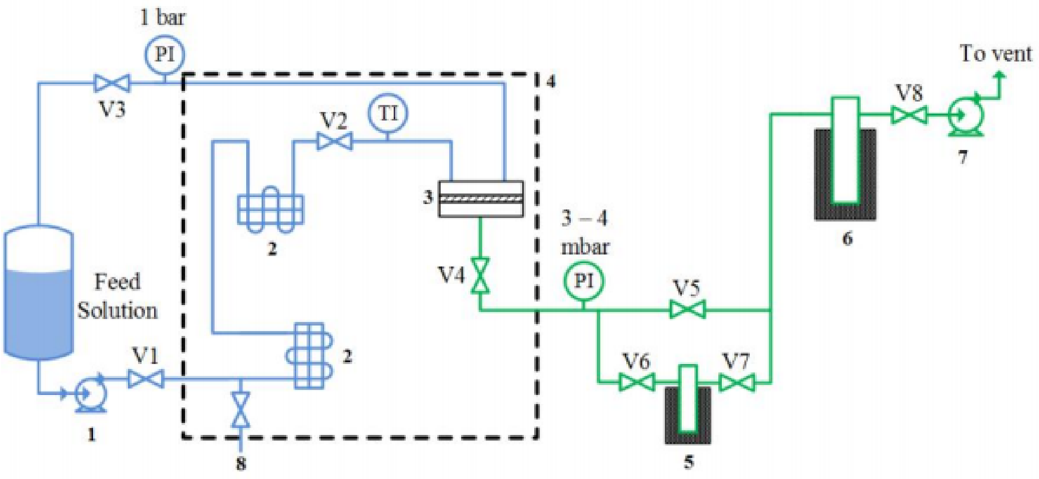

Figure 3.1: Flow sheet showing the pervaporation setup used in this project (Ansaloni et al., 2017a).

3.3.4 Titration

Each sample (0.2 mL) was diluted with DI water (50 mL) and titrated in a Mettler Toledo G20 compact titrator with 0.1 M H_2SO_4 until pH 2.5 was reached. For small concentrations of MEA, the samples were titrated with 0.01 M H_2SO_4. Each sample was examined twice in order to be sure that the results were correct. The concentrations were then calculated in a LabX titration software by Equation 3.1

$$Amine(mol/kg) = \frac{\mathrm{H_2SO_4(ml)} \cdot 0.2}{Sample(g)} \tag{3.1}$$

In case of the permeate samples from pervaporation of AF2400/XT-RGO the titrator could not detect the concentration, which is explained further in Appendix A. These samples therefore had to be examined by ion chromatography.

3.3.5 Ion chromatography

Each sample solution was diluted with water purified in a ICW-3000 (Millipore) to 1:10, 1:100, 1:1000 and 1:10000. Solutions from the permeate was only diluted to 1:1000. In addition, standard samples were prepared with 200, 100, 50, 20, 10, 5 and 2 ppm. The samples were then examined in a Thermo Scientific Dionex ICS-5000 ion chromotograph.

3.3.6 Mixed gas permeation

The CO_2 permeability and CO_2/N_2 selectivity were found by using a mixed gas separation setup shown in Figure 3.2. A circular cut of the membrane to be studied of 2.2 cm^2 with a thickness of approximately 50 μm was placed in the membrane module indicated in Figure 3.2. The feed gas was a mixture of 10% CO_2 and 90% N_2 of 1.6 bar, while the sweep gas was pure CH_4 of 1.05 bar. The feed flow was set at 400 mL/min and the sweep flow was set at 100 mL/min. Selectivity and permeability was measured based on information about pressure, humidity level, water pressure, flow, content in feed, retentate, permeate and membrane thickness. Pressure was measured by a pressure gauge, and relative humidity by a humidity detector. Flow was measured by an average of 5 bubble tests, and a gas chromatograph measured the content of CO_2, N_2 and CH_4 in both the permeate and the retentate. Each membrane was tested at three different humidity levels (0%, 50% and 100%) and three different temperatures (25°C, 40°C and 60°C).

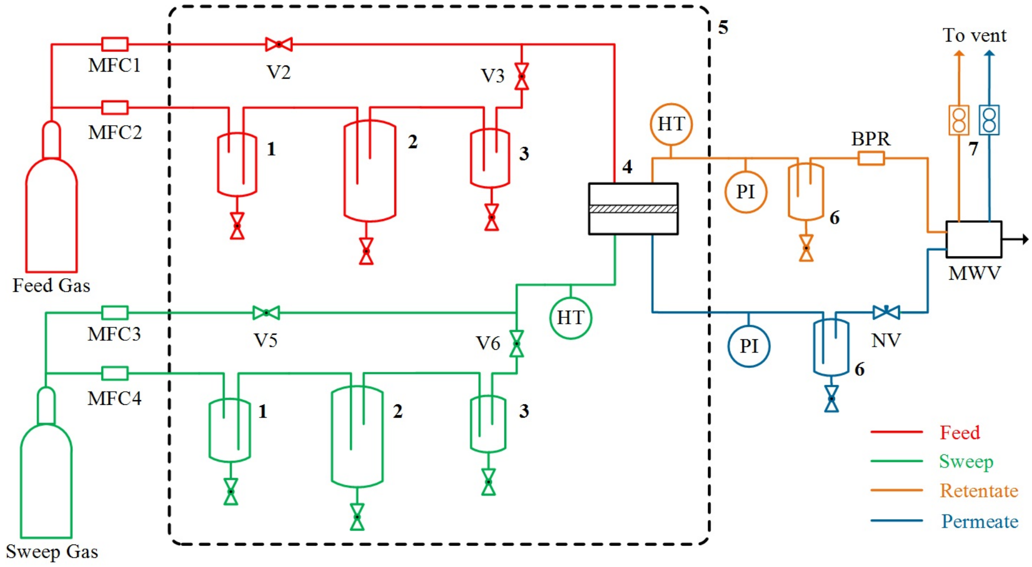

Figure 3.2: Flow sheet showing the mixed gas permeation setup. 1: Safety trap, 2: Humidifier, 3: Droplets trap, 4: Membrane module, 5: Heated cabinet, 6: Water knockout. MFC: Mass flow controller, NV: Needle valve, BPR: Back pressure regulator, PI: pressure indicator, HT: humidity and temperature sensor, MWV: Multi-way valve.

3.3.7 Membrane contactor study

A membrane with thickness of approximately 10 μm was placed in membrane cell indicated in Figure 3.3. The liquid flow was then set to 100 mL/min, adjusted by a pump set at 2380 rpm. Then a gas stream of 32 mL/min of CO_2 and 218 mL/min of N_2 was sent into the system. First, the gas stream was circulated in the system without being in touch with the absorbent for 40 minutes in order to measure the average CO_2 concentration before absorption. The CO_2 vol% was measured continuously by a gas chromatograph connected to the system. Before sending the gas stream into the absorption loop a bubble test was performed 5 times on the gas flow in order to measure the speed of the flow. After 1-1.5 hours the gas flow was measured again and the system was turned off. The absorbed amount of CO_2 was found from subtracting the average CO_2 stream after the gas stream was circulated with the absorbent from the average CO_2 stream before the gas stream came in contact with the absorbent. The test was performed at room temperature, 40°C and 60°C. The setup does not contain a stripper component, so this experiment only addresses the absorption of CO_2.

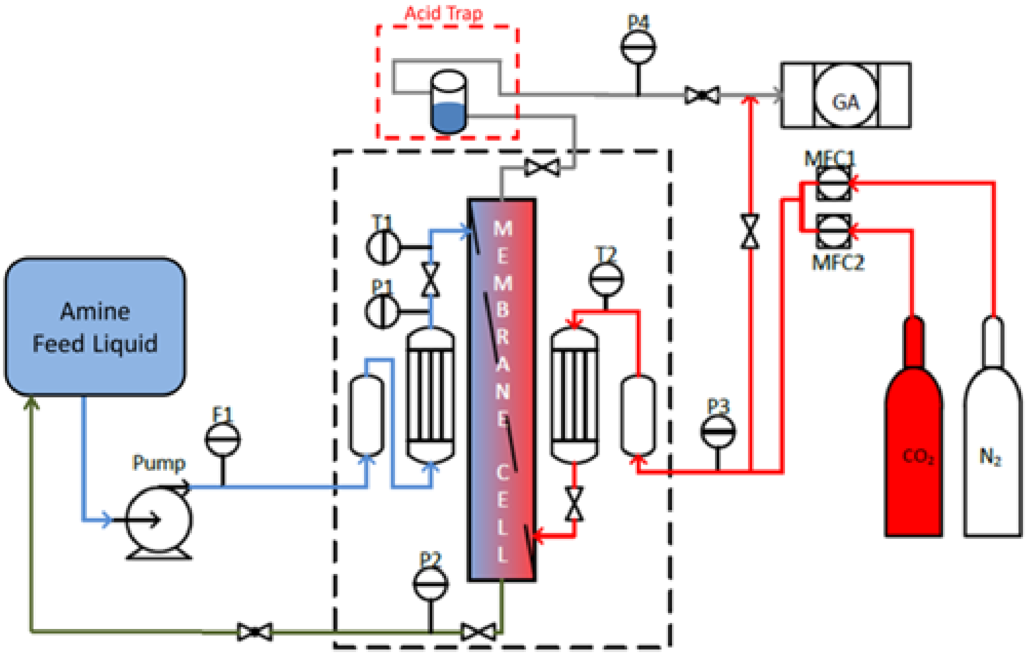

Figure 3.3: Flow sheet of the membrane contactor setup (Saeed and Deng, 2016).

3.4 Dip coating of hollow fibers

In order to find the optimal dipping conditions of AF2400 on tubular polypropylene (PP) fibers, three different sizes of tubular fibers were dipped once or twice for 10 seconds in different concentrated solutions of AF2400. The concentrations tested were 3.5 wt%, 2.5 wt% and 1.0 wt%. After dipping and drying, cross-sections of the tubular fibers were studied in a scanning electron microscope (SEM), TM3030PLUS (HITACHI) in order to find the thickness of the membrane layer. The SEM images were then analyzed in the software ImageJ, where 5 thickness measurements were taken from 4 different images of the fibers. The average thickness of these 20 measurements was considered the thickness.

4 Experimental results and discussion

The results from this section were obtained from experimental studies of self standing membranes. A later section will present a simulation study on membrane modules that was introduced in the theory section. Membrane modules are also addressed in this section, but only as an experimental study on dip coating techniques for optimization of layer thickness.

4.1 Nanocomposite membrane morphology

Photos of AF2400, AF2400/XT-RGO an AF2400/ZIF-8 are given in Appendix B. It is evident that the homogeneity in case of AF2400/ZIF-8 is not sufficient, as lighter patches are observed at the membrane surface. Pure AF2400 and AF2400/XT-RGO had a higher degree of homogeneity.

In order to analyze whether the addition of nanoparticle is compatible with the AF2400 polymer matrix, the nanocomposite membranes were studied in S(T)EM. Two S(T)EM images of the cross-section of AF2400/3wt% XT-RGO are shown in Figure 4.1.

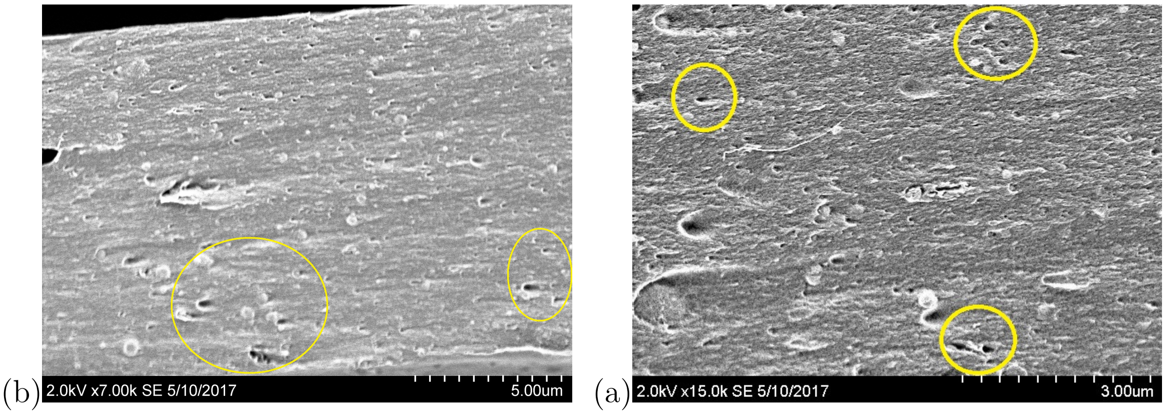

Figure 4.1: (a) Cross-section S(T)EM image of AF2400/3wt% XT-RGO at 7 000 magnification (b) Cross-section S(T)EM image of AF2400/3wt% XT-RGO at 15 000 magnification.

The surface of the cross-section indicates that the polymer + XT-RGO matrix is quite homogeneous. In both images there can be observed holes, indicated by the yellow circles. These holes can either be damages from the sample preparation or holes due to graphene layers in the polymer matrix. The XT-RGO particles are not directly visible at this magnification. This can either be explained by the fact that the particles are too small to be detected at this level of magnification, or that the particles are well immersed in the polymer matrix. It was not possible to magnify the image more, as the polymer phase started to melt at higher magnifications. The surface image of XT-RGO appeared similar to the pure polymer and is therefore not included in this thesis.

Two membrane cross-section S(T)EM images of AF2400/3wt% ZIF-8 are presented in Figure 4.2. The images are captured at the same magnification as the cross-section images of AF2400/XT-RGO.

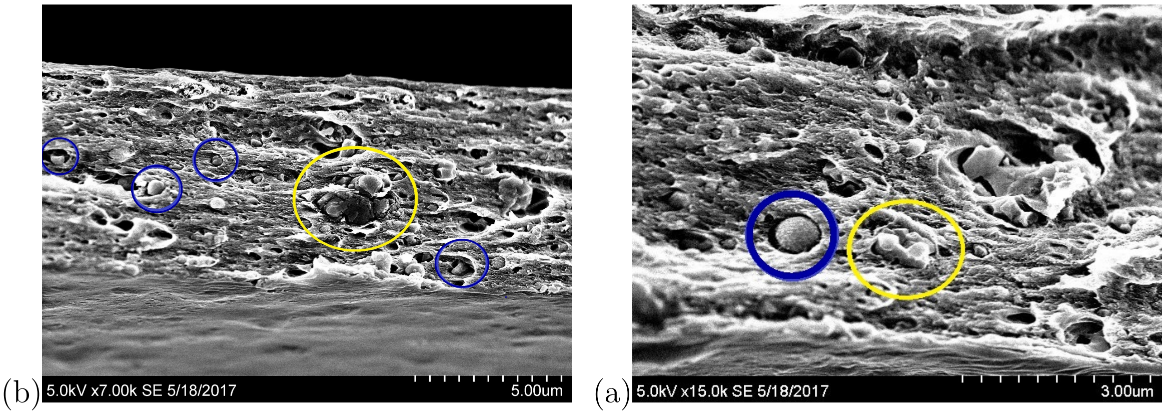

Figure 4.2: (a) Cross-section S(T)EM image of AF2400/3wt% ZIF-8 at 7 000 magnification (b) Cross-section S(T)EM image of AF2400/3wt% ZIF-8 at 15 000 magnification. The blue circles indicate sieve-in-cage voids and the yellow circles indicate nanoparticle clusters.

The cross-section of AF2400/3wt%ZIF-8 had a lower degree of homogeneity compared to AF2400/3wt%XT-RGO. In Figure 4.2, two yellow circles indicate clusters of ZIF-8 particles, and the blue circle indicate a sieve-in-cage hole. In the AF2400/XT-RGO surface image shown in Figure 4.3 it is also evident that some particles are clustered together in large groups. This implies that the membrane preparation of AF2400/ZIF-8 can be improved in order to increase the degree of homogeneity and the affinity between ZIF-8 and AF2400.

Contrary to AF2400/XT-RGO, the nanoparticles are visible in both cross-section images of AF2400/ZIF-8. The nanoparticle indicated by the blue circle in Figure 4.2 (b) has a measured diameter of approximately 500 nm, which confirms that the particles have nano scale dimensions.

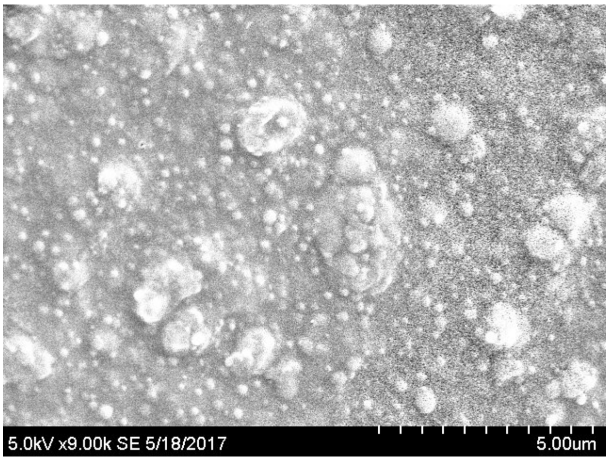

Figure 4.3: Surface S(T)EM image of a AF2400/3wt% ZIF-8 membrane.

4.2 Membrane compatibility study

In figures 4.4 to 4.7 the change in mass of PIM, PTMSP and AF2400 membranes when immersed in 3D3M, 3DEA2M, 3HEPP2M and MEA is shown. 6FDA-durene (a PI membrane) was also immersed in the amine solutions but dissolved after 24 hours in all cases. In Figure 4.8 the change in membrane mass when immersed in water is shown.

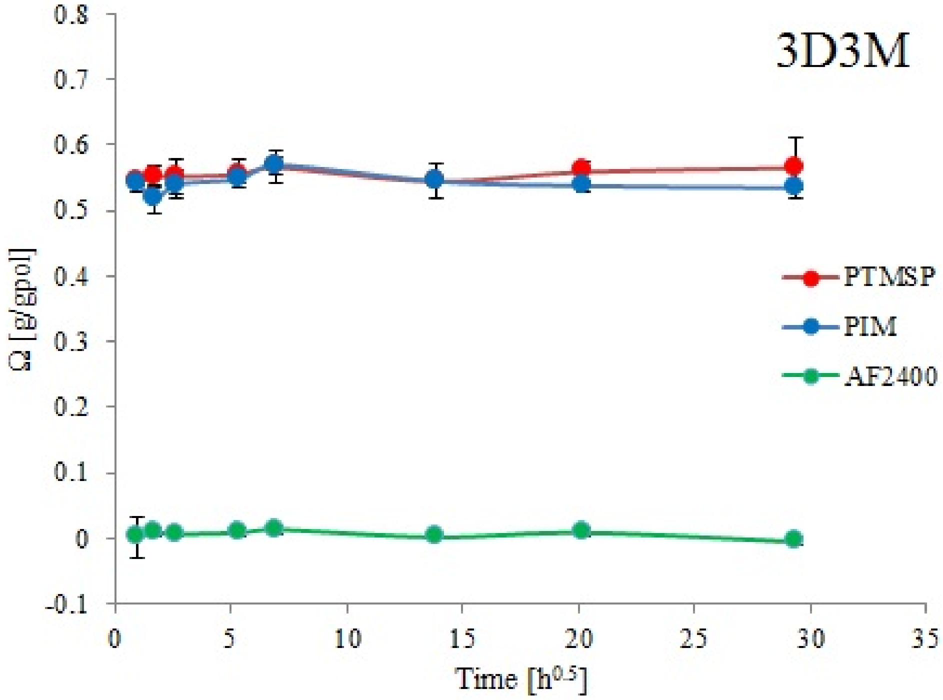

Figure 4.4: Development of weights of membrane pieces in a 3D3M solution.

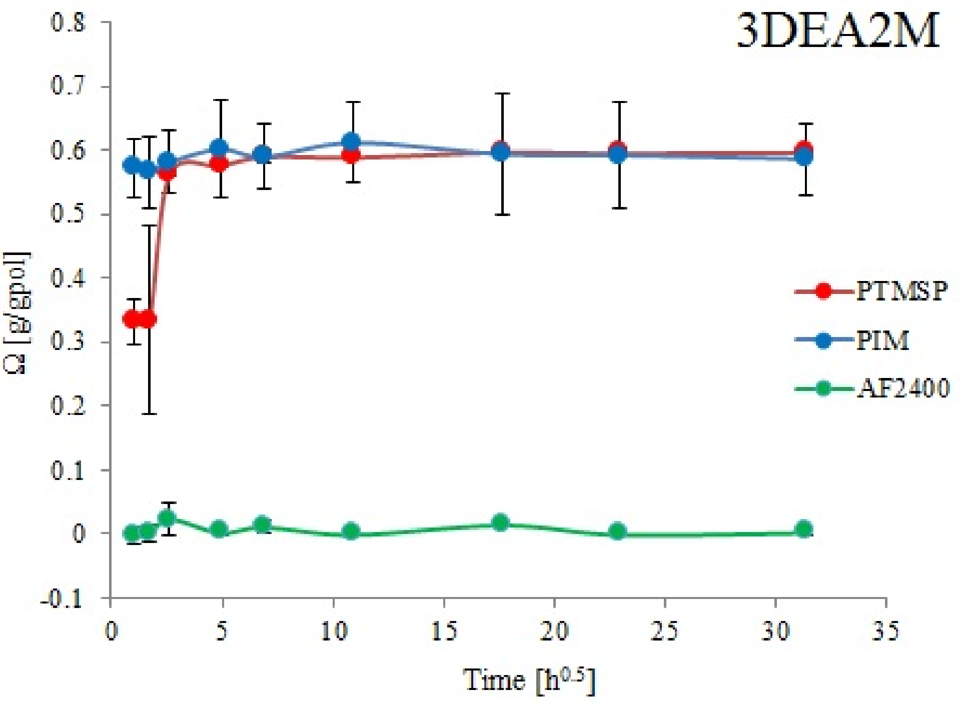

Figure 4.5: Development of weights of membrane pieces in a 3DEA2M solution.

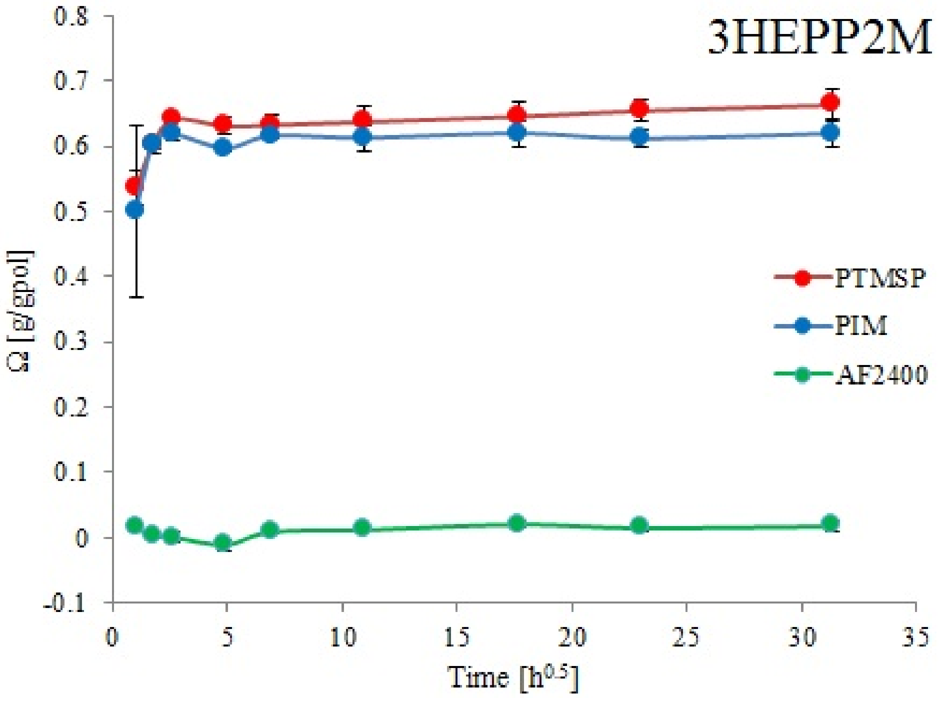

Figure 4.6: Development of weights of membrane pieces in a 3HEPP2M solution.

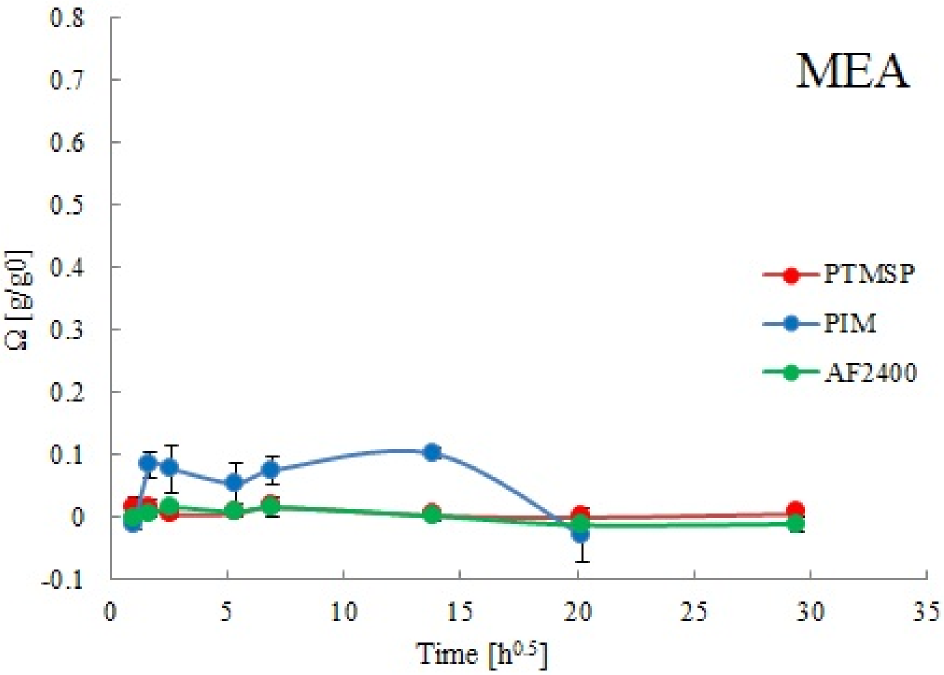

Figure 4.7: Development of weights of membrane pieces in a MEA solution.

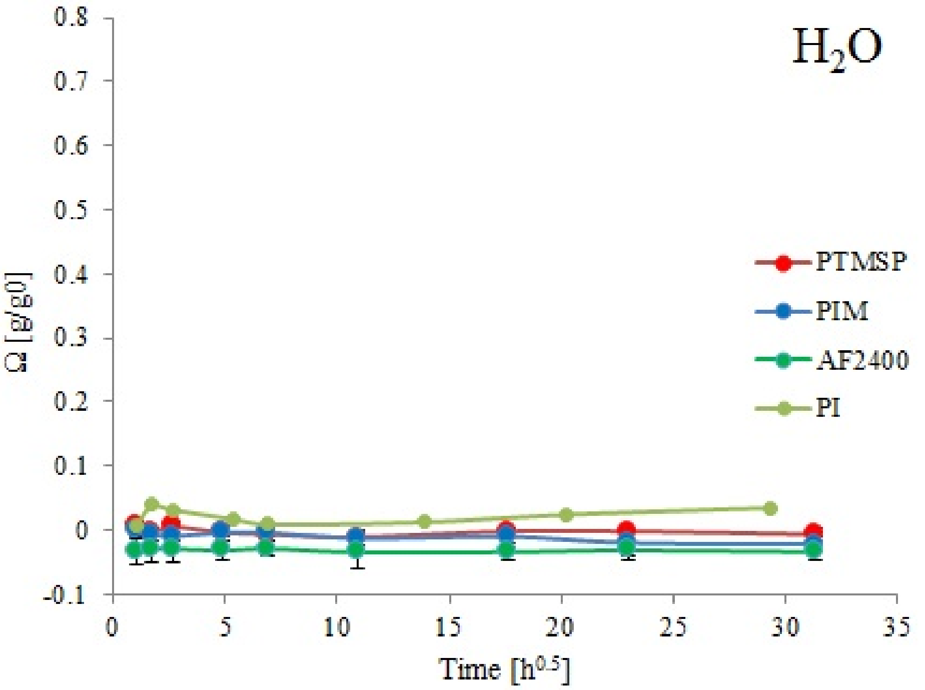

Figure 4.8: Development of weights of membrane pieces in a H_2O solution.

In all 3rd generation absorbents (3D3M, 3DEA2M and 3HEPP2M) AF2400 showed better stability compared to PTMSP, PIM and 6FDA-durene. In all cases AF2400 showed no significant change of weight, while for PTMSP and PIM it was observed a weight increase of 50-60%, and 6FDA-durene dissolved. In case of PTMSP and PIM immersed in 3DEA2M the error was quite large compared to the other results, but there was still a significant sign of absorption of solvent.

In case of MEA it was not observed any significant change of weight for PTMSP and AF2400. PIM did increase its weight with approximately 10% the first 16 days, but according to Figure 4.7 it decreased back to its initial weight after 35 days. This is a misleading indication because PIM proved to increase its fragility in both MEA, 3DEA2M, 3D3M and dissolved in many pieces which made it difficult to pick up all the membrane pieces from the solvent. The last measurement of PIM in MEA was impossible to weigh because the membrane was in too many pieces to pick all up from the solvent. Therefore the study of PIM in MEA should be repeated in order to conclude if there actually is a 10% permanent weight increase when immersed in MEA. Other inaccuracies in this study are connected to the fact that the initial weight could have included particles of dust that were washed off in the solvent, or that the membrane pieces were not dried well enough before weighing. This can result in a lower and higher degree of absorption respectively.

None of the membranes showed any significant change in weight when immersed in water. This is also the only fluid for which PI did not dissolve. All the absorbents were water diluted, so the fact that none of the membranes absorbed pure water indicate that it is the amines that are absorbed when a change in weight is observed.

AF2400 prove to be the most promising of the high free volume polymer membranes tested in terms of being implemented in a membrane contactor system with the new 3rd generation solvents (3D3M, 3DEA2M and 3HEPP2M) since it neither shows signs of absorption or dissolving when immersed in the absorbents.

4.3 CO_2 permeability

In order to study the CO_2 permeability of the nanocomposite membranes the membranes were studied in a mixed gas separation setup. In Figure 4.9 the measured CO_2 permeability of AF2400/ZIF-8 and AF2400/XT-RGO membranes are given at 0%, 50% and 100% relative humidity at room temperature, 40°C and 60°C, based on experiments in a mixed gas separation setup.

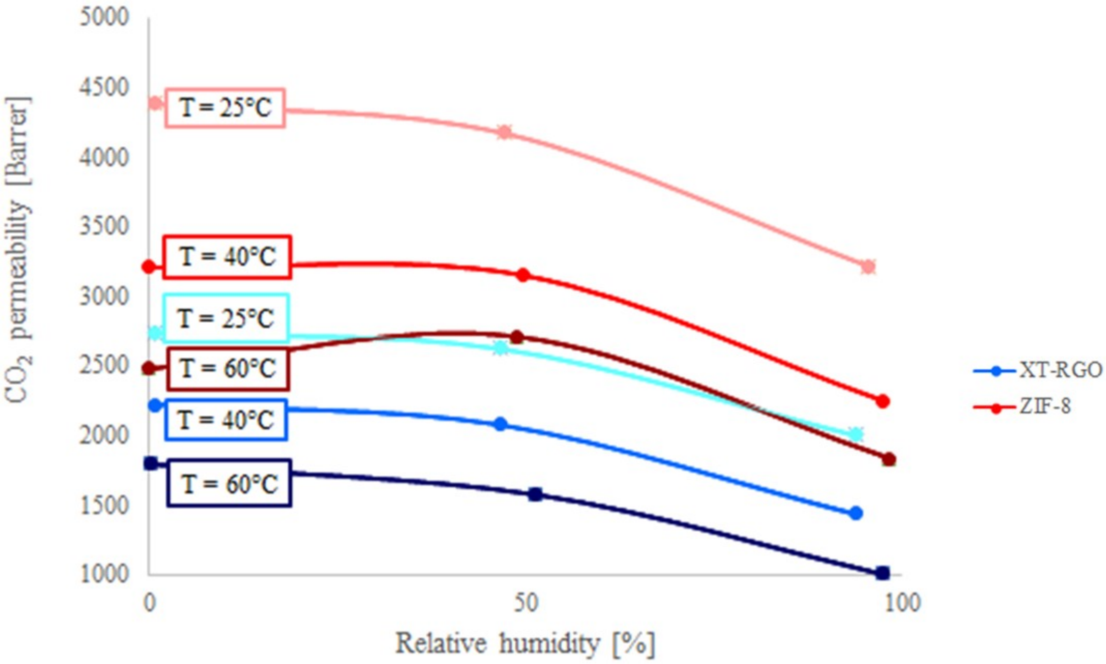

Figure 4.9: CO_2 permeabilities of nanocomposite AF2400 membranes at 25°C, 40°C and 60°C. The red nuances represent AF2400/ZIF-8 membranes and the blue nuances represent AF2400/XT-RGO membranes.

The AF2400/ZIF-8 membrane had a higher CO_2 permeability compared to the AF2400/XT-RGO membrane at all tested process temperatures. In addition, it was observed a decrease in permeability with both temperature and relative humidity in both membranes.

The separation factor of CO_2/N_2 is of less importance than the membrane selectivity of CO_2/absorbent, but can be an indicator of the general membrane selectivity. In Figure 4.10 the membrane separation factors of CO_2/N_2 is shown for AF2400/ZIF-8 and AF2400/XT-RGO depending on temperature and relative humidity.

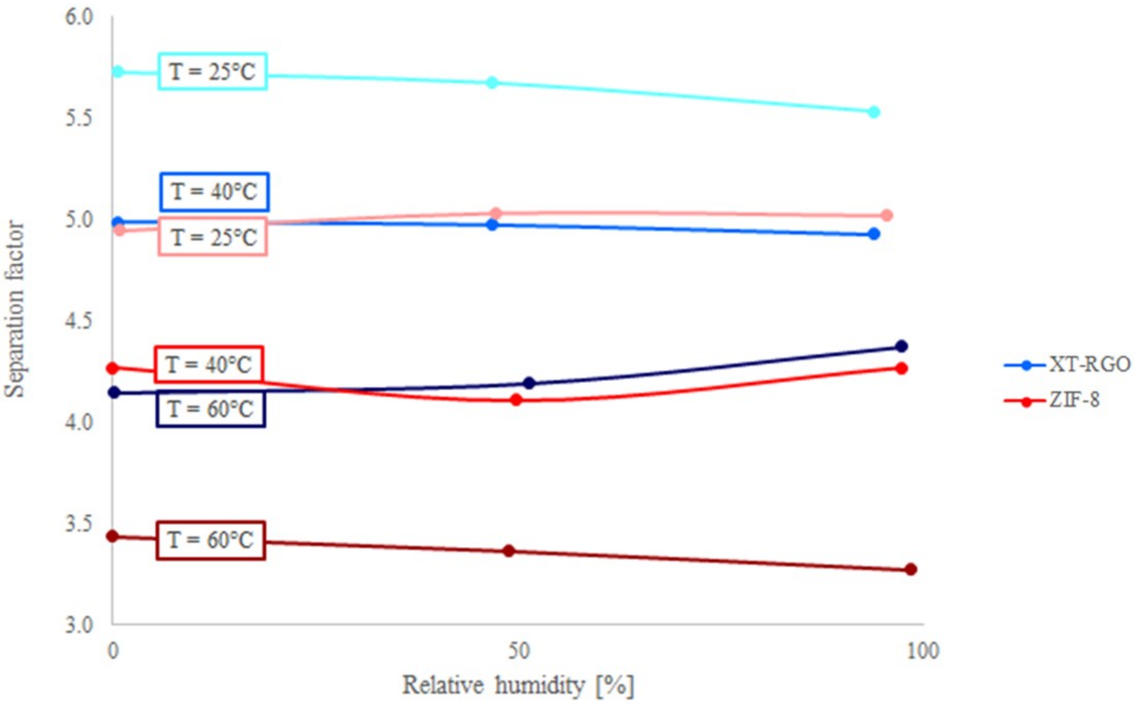

Figure 4.10: CO_2/N_2 separation factors of nanocomposite AF2400 membranes at 25°C, 40°C and 60°C. The red nuances represent AF2400/ZIF-8 membranes and the blue nuances represent AF2400/XT-RGO membranes.

The separation factor was higher for the AF2400/XT-RGO membrane compared to the AF2400/ZIF-8 membrane at the tested process temperatures. For both membranes it was observed a decrease in separation factor with increased temperature, while the impact of relative humidity was insignificant.

The fact that ZIF-8 contributed to a higher CO_2 permeability than XT-RGO can be explained by the morphology of the membrane matrix. In Figure 2.7 in Section 2.2.2 the sieving mechanisms for ZIF-8 and XT-RGO are given, and considering the fact that CO_2 is permeable through ZIF-8 particles and not through XT-RGO, it makes sense that addition of XT-RGO will give a lower CO_2 permeability compared to ZIF-8. In addition, the observed sieve-in-cage of the ZIF-8 structure will increase the permeability.

Compared to the CO_2 permeability of pure AF2400 (4800 Barrer), shown in Table 2.1 in Theory Section 2.2.2, none of the nanocomposite membranes managed to increase the CO_2 permeability. Nevertheless, a higher separation factor compared to pure AF2400 (4.1) was observed in all experiments except AF2400/ZIF-8 at 60°C.

The reason behind AF2400/ZIF-8 having a lower separation factor compared to AF2400/XT-RGO can be the observed sieve-in-cages and agglomeration of ZIF-8 particles in the S(T)EM cross-section image of AF2400/ZIF-8 in Section 4.1.

4.4 Amine evaporation

In order to study the evaporation of amines through each membrane, the membranes were tested in a membrane pervaporation setup. The permeability of amine solvents present the potential of amines to evaporate through the membrane in a membrane contactor setup. Results from the tests of AF2400 + XT-RGO and AF2400 + ZIF-8 are presented together with results from pure AF2400 membrane in Figure 4.11, as an average of 3 measurements. Results from the pure polymeric membrane were provided by Dr. Luca Ansaloni. The value for MEA permeability through pure AF2400 was interpolated by a power regression line of permeability values at 25°C, 40°C and 60°C, and error bars are therefore not included at this datapoint.

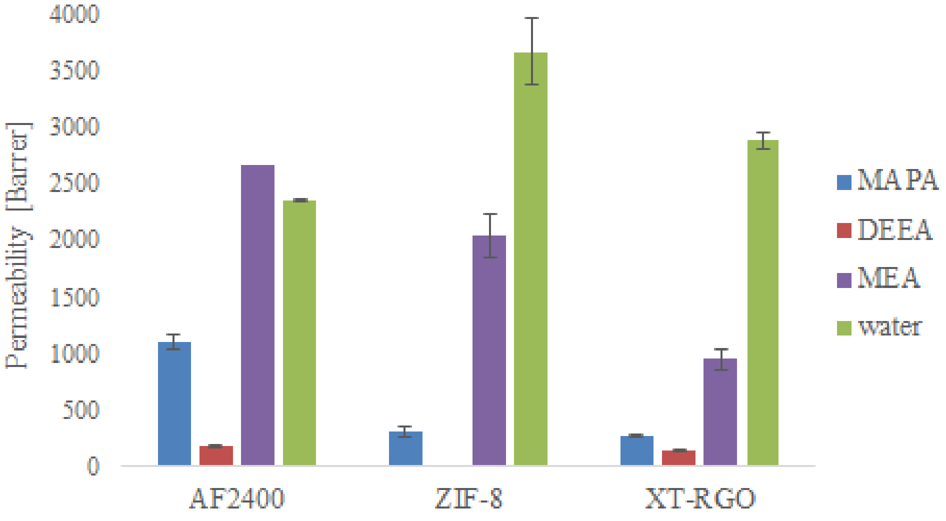

Figure 4.11: Amine evaporation trough pure polymer membrane and nanocomposite membranes at 50°C.

In case of MAPA the permeability was significantly lower for both AF2400/ZIF-8 and AF2400/XT-RGO compared to the pure polymeric AF2400 membrane. In both types of mixed matrix membranes a reduction of approximately 70% Barrer was observed compared to the pure AF2400 membrane.

The permeability of DEEA was significantly lower in all three types of membranes compared to MAPA. This coincides with the fact that DEEA is a branched amine, and hence a molecule with larger size MAPA, which has a more linear structure. In case of glassy polymers, the larger a molecule is, the harder it is for the molecule to permeate.

The reduction of permeability of DEEA was a bit low in XT-RGO embedded membranes compared to the pure polymeric membrane, approximately 20%. In case of ZIF-8 the reduction was quite significant - approximately 98%.

The prevention of MEA permeability was not very high in case of the AF2400/ZIF-8 membrane compared to the pure AF2400 membrane, approximately 20%. In case of AF2400/XT-RGO the permeability decreased by approximately 60% compared to the pure polymeric membrane, and thereby RGO performed better than ZIF-8. Nevertheless, the permeability of MEA was higher than MAPA and DEEA in case of both nanocomposite membranes. This can be explained by the fact MEA is a smaller molecule than MAPA and DEEA.

None of the nanocomposite membranes have consistently higher amine permeability compared to the other one. ZIF-8 is hydrophobic, while XT-RGO is more hydrophobic proportionally with the amount of reduced oxygen atoms. The interaction between the nanoparticles and absorbents can be studied further in order to understand the differences in amine permeability across the membranes.

The permeability of water was a lot higher in the nanocomposite membranes compared to the permeability of absorbents. This is because despite ZIF-8 and XT-RGO are hydrophobic, they are more hydrophilic than AF2400. This is a significant observation due to its effect of the long term concentration of absorbents in a continuous membrane contactor process. This means that either water needs to be added to the absorbent flow or the feed stream of gas needs to be saturated with water in order to decrease the driving force of water.

These results prove that adding nanoparticles to the membrane matrix do reduce the evaporation of MAPA and DEEA (3D3M) and MEA. The membrane matrix with ZIF-8 proved to most efficiently reduce the permeability of DEEA, while the permeability of MAPA was reduced approximately to the same extent in both nanocomposite membranes. MEA had a higher prevention of permeability in the AF2400/XT-RGO membrane.

4.4.1 CO_2/amine selectivity

The selectivity of a membrane does not solely depend on the permeability of compounds, but also the flux, which in Equation 2.3 is given as the permeabiltiy multiplied with the partial pressure difference across the membrane. This implies that factors affecting the partial pressure, such as activity coefficients and molar fractions also affect the selectivity. In Figure 4.12 the CO_2/amine selectivity of the two nanocomposite membranes are given at 50°C for MEA, DEEA and MAPA. The calculation behind the selectivity values is shown in Appendix C.

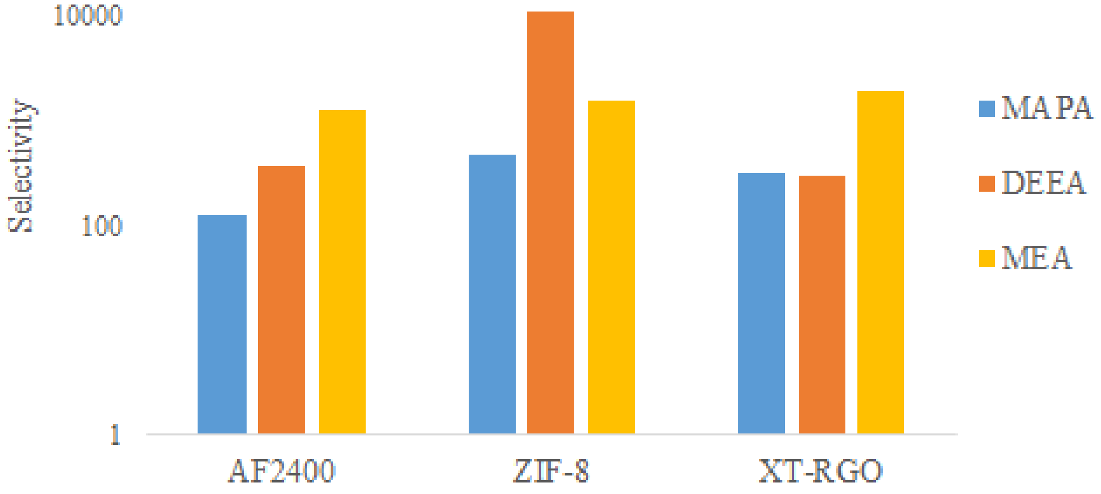

Figure 4.12: CO_2/amine selectivity of AF2400/ZIF-8, AF2400/XT-RGO and pure AF2400 membranes at 50°C.

Even though the permeability of MEA was higher compared to MAPA and DEEA in both AF2400/ZIF-8 and AF2400/XT-RGO, MEA had higher CO_2 selectivity compared to MAPA and DEEA in the AF2400/XT-RGO membrane, due to a one order of magnitude lower Δp in case of MEA. This is in turn resulting in a lower driving force of MEA compared to DEEA and MAPA.

In the AF2400/XT-RGO membrane the MEA permeability was approximately five times larger than the MAPA permeability, but the CO_2/MEA selectivity was approximately 6 times larger than the CO_2/MAPA selectivity. This coincides with the Δp_i values of MEA and MAPA shown in Table C.5 in Appendix C, where Δp_{MEA} is one order of magnitude lower than Δp_{3D3M}.

In the AF2400/ZIF-8 membrane the selectivity of DEEA was significantly higher than the selectivity of MAPA and MEA. This is a result of the DEEA permeability trough AF2400/ZIF-8 being extremely low compared to the other amine permeabilities.

Both nanocomposite increase the selectivity of CO_2/amine except the CO_2/DEEA selectivity of XT-RGO which is slightly lower compared to pure AF2400. The most significant increase in selectivity is observed in the AF2400/ZIF-8 membrane where the CO_2/DEEA selectivity is increased by 10800.

The CO_2/N_2 separation factor was proven to be higher for AF2400/XT-RGO than AF2400/ZIF-8 in Section 4.3. In case of amines, the selectivity is not consistently higher for one membrane compared to another, so the CO_2/N_2 separation factor does not work very well as an indicator on the amine separation. Also, in sum, AF2400/ZIF-8 has a higher amine selectivity compared to AF2400/XT-RGO, which is a contradiction to the results related to the CO_2/N_2 separation factor.

4.5 Membrane contactor results

In this section, final investigation on how AF2400/XT-RGO and AF2400/ZIF-8 perform in an actual membrane contactor is presented. The amine emission is not known in this study, so the emission is assumed from the pervaporation study.

In Figure 4.13 the measured CO_2 permeability of AF2400/ZIF-8 and AF2400/XT-RGO is presented with its effect of temperature increase. The CO_2 permeability of pure AF2400 was provided by Dr. Luca Ansaloni (NTNU).

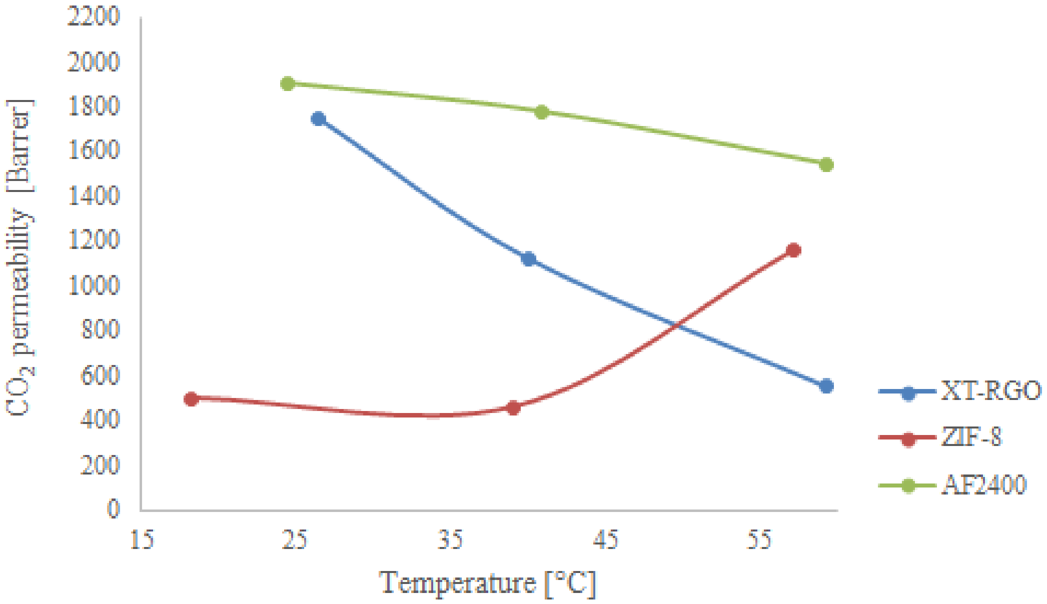

Figure 4.13: CO_2 permeability for AF2400/XT-RGO, AF2400/ZIF-8 and pure AF2400 in membrane contactor.

The permeability of CO_2 in case of AF2400/XT-RGO presented the same development with respect to temperature as in the mixed gas experiment results in Section 4.3, whereas the permeability of AF2400/ZIF-8 characterized a different temperature development compared to the mixed gas results.

At lower temperatures (room temperature and 40°C) the CO_2 permeability of ZIF-8 was only approximately 400-500 Barrer, which is significantly lower than the XT-RGO membrane with permeabilities between 1700 - 1100 Barrer at the same temperatures. At 60°C, the permeability of the XT-RGO membrane decreased additionally, while the ZIF-8 membrane increased its permeability almost by a double. Since the results of the ZIF-8 membrane can be considered unexpected, the test was repeated. However, this showed no improvements in the performance of the membrane. This can be explained by errors in the system, or it can be effects of temperature on the ZIF-8 particles in the membrane matrix. It can also be explained by the morphology of the nanocompsite membranes, which had both observed sieve-in-cage and agglomeration of nanoparticles.

In Figure 4.14 CO_2 permeabilities through AF2400/XT-RGO membranes from membrane contactor and mixed gas experiments are given at room temperature, 40°C and 60°C.

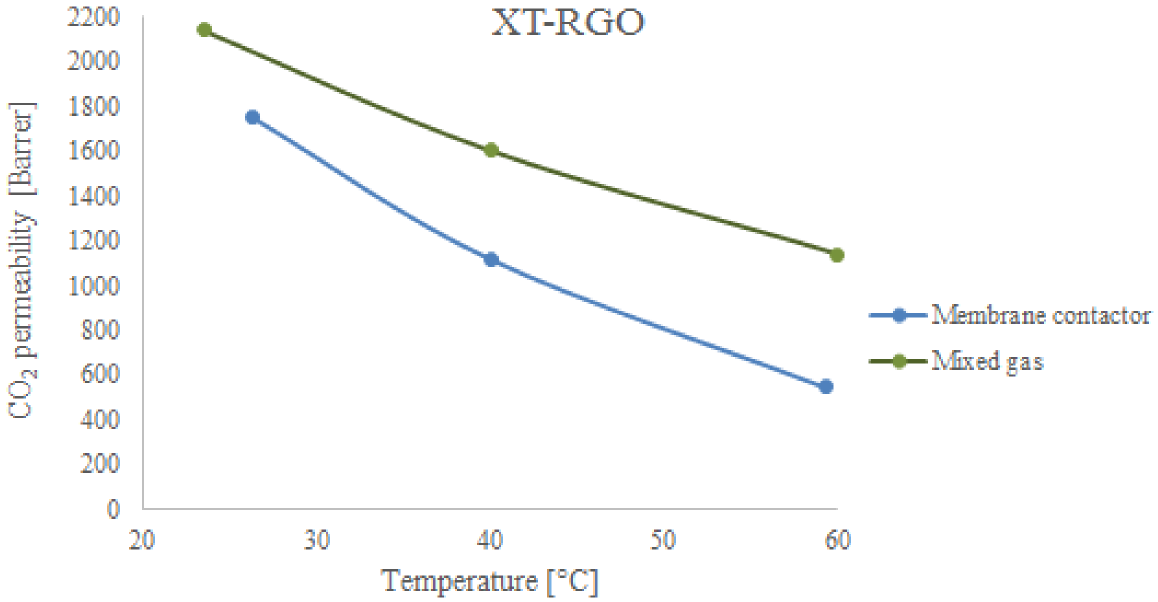

Figure 4.14: CO_2 permeability for AF2400/XT-RGO from mixed gas membrane contactor studies.

It is evident from the figure that the CO_2 permeability is lower in the membrane contactor experiment compared to the mixed gas experiment. The membrane amss transfer resistance is the same, but in the membrane contactor an additional mass transfer resistance is added by the liquid absorbent, as mentioned in Equation 2.7 in Section 2.4.1.

The difference in mixed gas and membrane contactor CO_2 permeability increased slightly with temperature. Considering the fact that the absorbent liquid become less viscous at higher temperatures, and that the mass transfer resistance decreases with decreasing liquid viscosity, the difference in performance between membrane contactor and mixed gas should decrease with temperature. Hence, the difference in CO_2 permeability can not be solely explained by the mass transfer resistance of the liquid absorbent, since there is observed an increase in the difference between permeability of mixed gas and of the membrane contactor.

The CO_2 permeability is lower in both nanocomposite membranes compared to pure AF2400, as was the case in the mixed gas experiments. Pure AF2400 also experienced a decrease in permeability with temperature, supporting the theory that the AF2400/ZIF-8 experiment is odd. Despite the fact that XT-RGO is extremely thermal stable, it is observed a faster rate of decrease of permeability in the AF2400/XT-RGO membrane compared to pure AF2400. This might imply that the affinity between AF2400 and XT-RGO is somehow affected by the temperature.

4.5.1 CO_2/amine selectivity

Knowing the CO_2 permeability through the nanocomposite membranes in an actual membrane contactor, it is possible to calculate the actual CO_2/amine selectivty of the membrane contactor. The permeability of amines will in reality be lower, due to a reduced volatility in CO_2 saturated amines. The procedure of calculating the selectivity is the same as in Section 4.3. The only difference is that the CO_2 permeability is calculated from an interpolation of a polynomial regression line of the CO_2 flux through AF2400/ZIF-8 and AF2400 and a linear regression of the CO_2 flux through AF2400/XT-RGO. The resulting selectivity values are given in Figure 4.15 below.

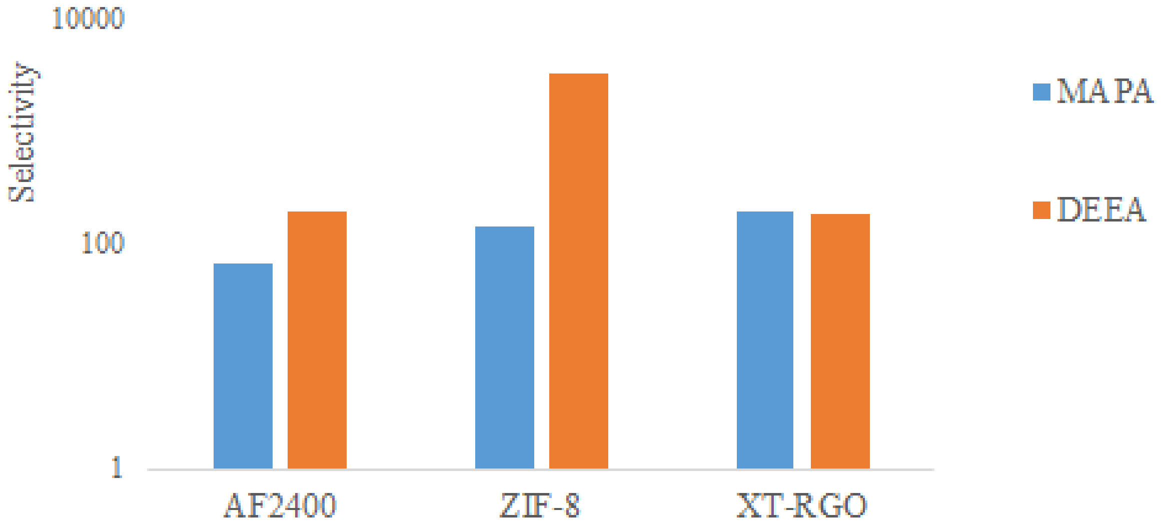

Figure 4.15: CO_2/amine selectivity in membrane contactor of AF2400/ZIF-8, AF2400/XT-RGO and pure AF2400 at 50°C.

Compared to the results from the mixed gas experiment, the CO_2/amine selectivity is lower in the membrane contactor. This follows the observation of decrease in CO_2 permeability in the membrane contactor compared to in mixed gas.

AF2400/ZIF-8 went from having a better CO_2/MAPA selectivity in mixed gas compared to AF2400/XT-RGO to the opposite in the membrane contactor - a higher CO_2/MAPA selectivity in AF2400/XT-RGO. In addition, the CO_2/DEEA selectivity of AF2400/ZIF-8 is decreased with 8000 in the membrane contactor compared to mixed gas.

The CO_2/MAPA selectivity is still higher in case of pure AF2400 compared to AF2400/XT-RGO. Overall, AF2400/XT-RGO has the highest selectivity of CO_2/MAPA, and the lowest selectivity of CO_2/DEEA out of the three membranes.

Considering the unexpected behaviour of the AF2400/ZIF-8 membrane, it is questionable whether the membrane is suitable in membrane contactors. AF2400/XT-RGO has in turn a more stable behaviour, but a lower CO_2/amine selectivity compared to AF2400/ZIF-8. The volatility of CO_2 saturated amines is unknown, but literature reports that the CO_2 saturation decreases the amine volatility. It is not known to which degree the amine permeability will decrease with CO_2 saturation indicating that the real selectivity can higher.

4.6 Dip coating characteristics

In figures 4.16 - 4.18 the measured thickness of AF2400 layer on hollow fiber polypropylene is shown depending on amount of dips and concentration of AF2400 in the dipping solution. This study was performed in order to understand how to dip fibers for membrane modules optimally. Optimally in this case means a low and homogeneous thickness of the membrane layer.

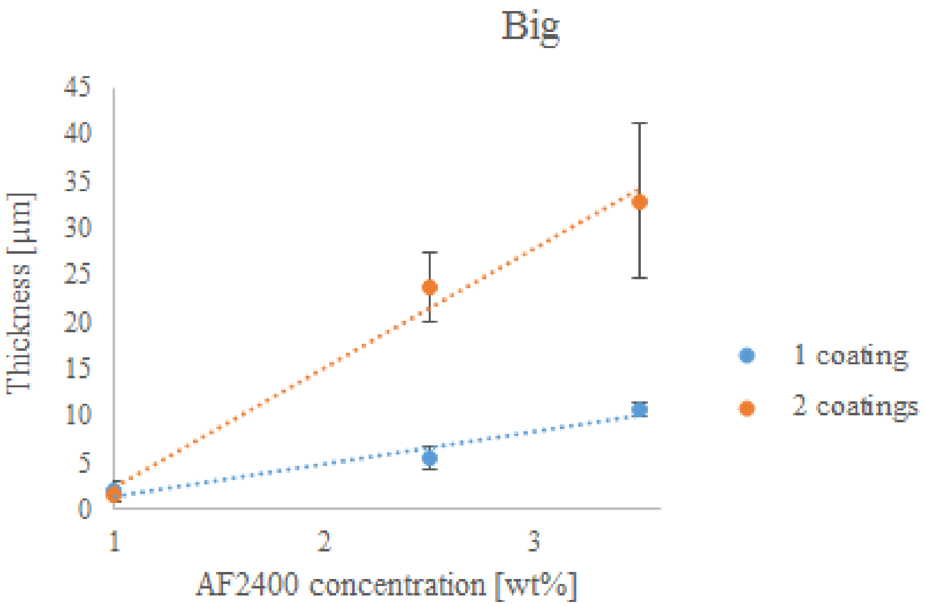

Figure 4.16: AF2400 thickness layer of big sized polypropylene hollow fibers.

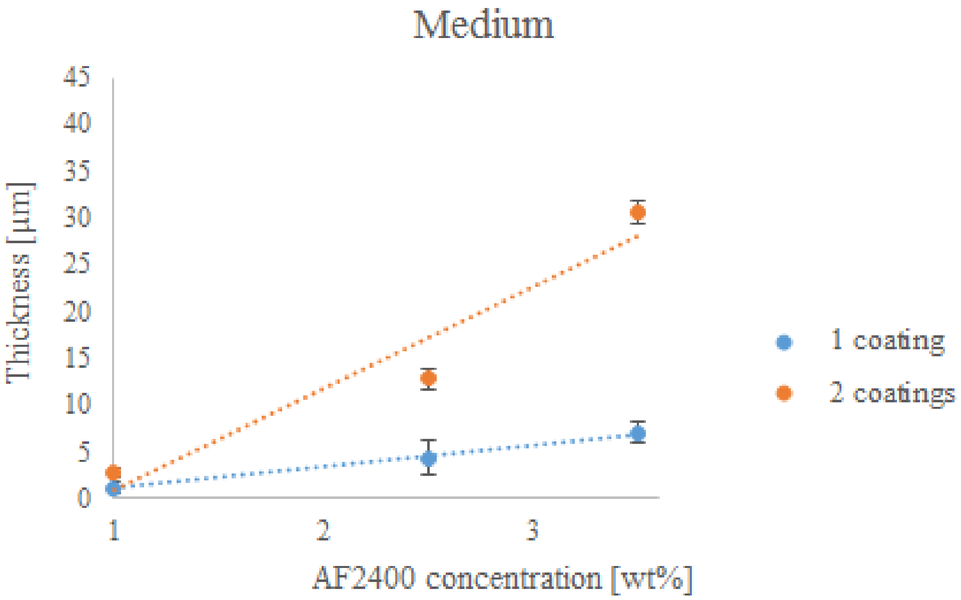

Figure 4.17: AF2400 thickness layer of medium sized polypropylene hollow fibers.

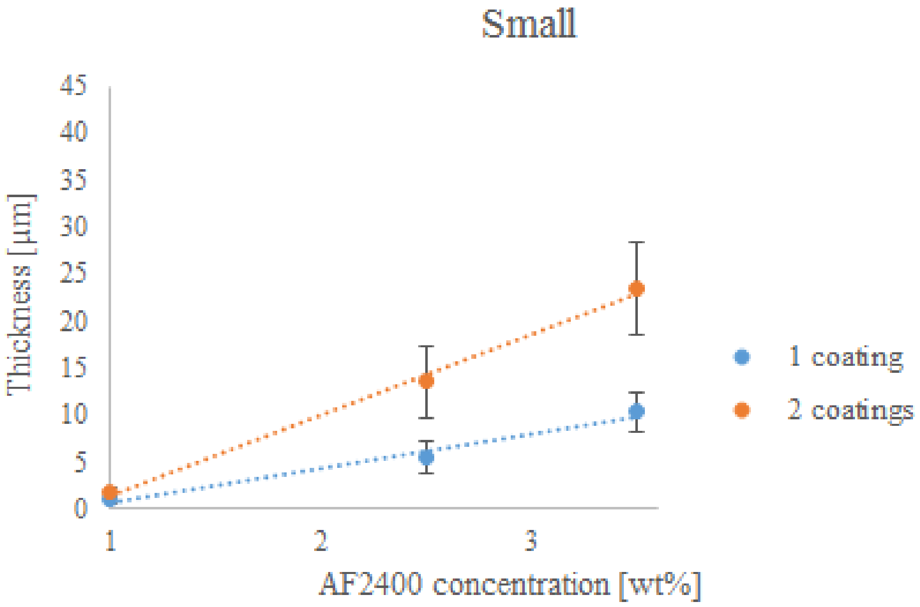

Figure 4.18: AF2400 thickness layer of small sized polypropylene hollow fibers.

In all three sizes of hollow fibers, the membrane layer was just slightly thicker for the fibers dipped twice in the 1.0 wt% AF2400 solution than the fibers dipped once. Then for all three sizes, the thickness was a lot higher for the fibers dipped twice in 2.5 wt% and 3.5 wt% solution compared to the fibers dipped once. This is because the thickness increased with increasing AF2400 concentration, and the thickness from the 1.0 wt%

solution was so thin that a second dip did not affect the thickness much. In Table 4.1 the interpolated concentration corresponding to 2 μm thickness is given for all three sizes of fibers, and number of dips.

Table 4.1: Interpolation table of membrane thickness. a and b are parameters from y = ax +b linear regression of datapoints in figures 4.16 - 4.18. The desired thickness/y-value is 2 μm and the wt% value is the concentration that interpolates to 2 μm.

Fiber size	# dips	a [μm/wt%]	b [wt%]	R^2	wt%
Small	1	3.69	-3.02	0.984	1.36
Small	2	8.58	-7.13	0.996	1.06
Medium	1	2.31	-1.20	0.996	1.35
Medium	2	10.8	-9.79	0.928	1.09
Big	1	3.40	-1.92	0.947	1.15
Big	2	12.8	-10.4	0.986	0.973

The R^2 value for some of the measurements indicate some inaccuracy in linearizing the datapoints which can also be seen from the error bars, while most of the R^2 values confirm that it is most likely correct to draw a linear trendline between the datapoints.

Normally, a tickness of 1 μm would be preferred, but in this case 2 μm was chosen based on the fact that it seemed more probable that the fiber would be fully covered of the AF2400 layer if the thickness was higher than 1 μm.

In Appendix D it is shown that the coating of small fibers were hard to make optimal, as gaps between coated layer and fiber were observed in almost all cases. It should be noted that the cross-sections of the hollow fibers were hard to make smooth, which can have resulted in gaps. The coating of medium fiber also proved to be difficult to optimize, while big fibers in all cases had a nice coating. This implies that manual coating big sized hollow fibers is feasible.

5 Modelling

The membranes studied in this thesis so far are self standing membranes, while in reality membranes will be applied as membrane modules which are described in the theory section. In the following section, a simple MATLAB model provided by PhD candidate Kristin Dalane for a membrane module applied as a membrane contactor is described and simulated in order to understand which parameters that are important to consider when engineering a membrane module for membrane contactor applications. The most important factor of this study is the loss of amines, as this is a parameter that is important to diminish. Another important factor is the surface area of the process, which describes the feasibility of the process. The model is simple, and is originally based on MEA as absorbent. The model is under development, so later the experimental results from this thesis can be implemented in a model for nanocomposite membranes of AF2400 and 3rd generation solvents.

5.1 Model theory

The simple model describes a counter-current flow of MEA and a gas stream of 13 mol% CO_2 and 87 mol% N_2 through tubular membrane modules bundled together in one tube. The model is further based on a few assumptions:

- Constant temperature and total pressure on feed and permeate side.
- All fibers perform equally.
- Water permeation is not considered.
- Only the retentate side is evaluated for MEA.
- Plug flow in the tubes
- The dense coating of the composite membrane resistance is the main resistance, assuming liquid and gas resistance are negligible.
- Constant total concentration of MEA in liquid phase.
- Constant liquid flow.

The model is set to have a constant removal of CO_2 at 90% of the inlet concentration, meaning that the CO_2 concentration in the outlet will be 1.3 mol%. This means that if a parameter that affects the removal efficiency of CO_2 is changed, the number of modules required to meet the demand of CO2 removal will be changed.

Liquid loading is a measure of how efficient the absorption of CO_2 is in case of a given absorbent. The liquid loading of MEA, ξ, is like the CO_2 removal set to be constant, shown in Equation 5.1:

$$\xi = \frac{\mathrm{CO}_{2out,l}[mol/s]}{MEA_{in,l}[mol/s]} \tag{5.1}$$

Where $CO_{2out,l}$ is the molar flow of CO_2 in the liquid outlet stream, and $MEA_{in,l}$ is the molar flow of MEA in the liquid inlet stream. This implies that the gas flow has to be modified relative to the liquid flow. ξ is in this model set to be constant at 0.42.

The parameters that are not kept constant, i.e defined as input parameters of the model are shown in Table 5.1:

Table 5.1: Input parameters to the model.

Input parameter	Symbol	Unit
Tube length	L	m
Tube diameter	d	m
Liquid film around tube	dxliq	m
CO_2 permeance	kCO2	$kmol/m^2sbar$
MEA permeance	kMEA	$kmol/m^2sbar$
Total pressure on feed side	Pf	bar
Total gas flow	Qg	$kmol/s$
Liquid volume flow	volL	L/s
Liquid temperature	Tl	^oC
Liquid weight fraction, MEA	wMEA	-
Liquid concentration, MEA	cMEA0	mol/L

Based on these input parameters, the model delivers the output parameters shown in Table 5.2.

The input parameter kMEA is in reality adjusted based on another parameter; the membrane selectivity ($\alpha_{CO_2/amine}$) of CO_2 and MEA, shown in Equation 5.2:

$$\alpha_{CO_2/amine} = \frac{J_{CO_2}}{J_{MEA}} \tag{5.2}$$

Where J_{CO_2} and J_{MEA} are the flux of CO_2 and MEA respectively. This means that the permeance of MEA is changed when the permeance of CO_2 is held constant in order to meet the selectivity demand. The CO_2 and MEA permeance for AF2400 membranes is a fixed value, implying that when these adjustments are performed it is considered a hypothetical membrane with the given permeance characteristics.

Table 5.2: Output parameters from the model.

Output parameter	Symbol	Unit
Molflow of CO_2 in retentate	nR	kmol/s
Molflow of CO_2 in permeate	nP	kmol/s
Mol% CO_2 in retentate	yCO2plot	-
Molflow of MEA in retentate	nR_e	kmol/s
Mol% of MEA in retentate	yMEA	-
Partial pressure of MEA in gas phase in equilibrium with MEA in liquid phase	pMEA0	bar

The parameter η is chosen as a measure of prevention of amine emission compared to conventional CO_2 absorption and is defined by Equation 5.3:

$$\eta = 1 - \frac{yMEA}{pMEA0} \cdot p_{tot} \tag{5.3}$$

5.2 Simulation results

In Appendix E it is shown that neither tube length, tube diameter, liquid film around the tube, total gas flow/liquid volume flow have any effect on η. Among the listed input parameters, only total gas flow/liquid volume flow has an impact on the total surface area. In this section all these input parameters are kept constant at values given in Table 5.3:

Table 5.3: Values of input parameters kept constant during this sensitivity analysis if nothing else is specified. The permeance value of CO_2 corresponds to 1000 Barrer.

Input parameter	Value	Unit
L	0.5	m
d	300	μm
dxliq	100	μm
Qg	23.26	$kmol/s$
volL	1300	L/s
Pf	1.1	bar
kCO2	3.50e-4	$kmol/m^2 sbar$

In Figure 5.1 the total membrane module surface area is plotted against liquid temperature for three different values of CO_2 permeability at α constant = 500. From the figure it is evident that temperature does not affect the surface area. Also, the surface area depends on the membrane permeability of CO_2, more specifically is the surface area inverse proportional to CO_2 permeability. It was also observed that the CO_2 permeability did not affect the prevention of amine emissions.

Considering the values in Table 5.3 the CO_2 permeability has to be high in order for the process to be feasible. The surface area values in Figure 5.1 correspond to $3.02 \cdot 10^8$ - $3 \cdot 10^{10}$modules. The tube length can be extended to some degree, but still the process unit will be enormous if the permeability is too low. Thus the higher CO_2 permeability, the more feasible process. AF2400 membranes have a CO_2 permeability in the range of 1000, meaning that the surface area of a membrane contactor setup with MEA as absorbent will be 10^6 m^2 and have $3 \cdot 10^9$ tubes, which is challenging to make feasible.

PIM and PTMSP are polymers known for their high CO_2 permeability. In Section 4.2 it was concluded that both PTMSP and AF2400 membranes are chemically compatible with MEA, so it could be a solution to substitute AF2400 with PTMSP in case of MEA absorption. In case of the 3rd generation solvents, neither PIM or PTMSP are compatible, whereas AF2400 is. It can not yet be concluded if AF2400 and 3rd generation solvents make a feasible process, as the VLE data for the solvents needs to be implemented in the model.

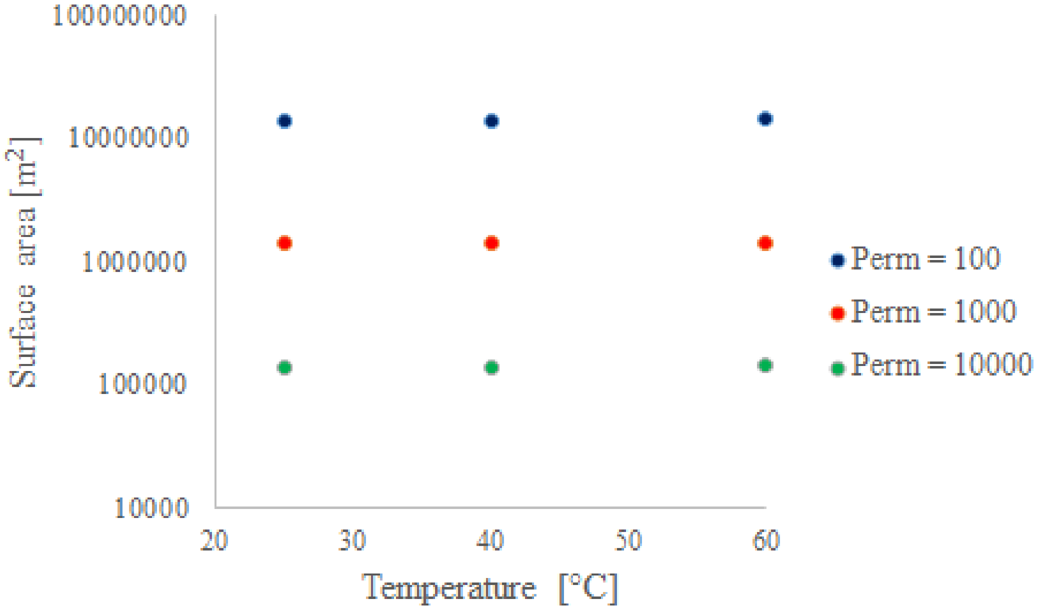

Figure 5.1: Effect of temperature and CO_2 permeability on membrane module surface area.

In Figure 5.2 the effect of temperature and membrane selectivity on prevention of MEA emissions, η is presented. In contrast to Figure 5.1 the relation between temperature and selectivity on η is not linear, which why several values of selectivity are shown.

From Section 4.5 the CO_2/amine selectivity of AF2400 nanocompsoite memembranes in membrane contactor is listed in Table 5.4:

Table 5.4: CO_2/amine selectivity of AF2400/ZIF-8 and AF2400/XT-RGO.

Membrane	Absorbent	Selectivity
XT-RGO	MEA	1385
ZIF-8	MEA	518
XT-RGO	MAPA	191
ZIF-8	MAPA	139
XT-RGO	DEEA	178
ZIF-8	DEEA	3258

Figure 5.2 is based on VLE data for MEA, and based on numbers in Table 5.4 AF2400/XT-RGO is better suited in membrane contactors compared to AF2400/ZIF-8, due to a higher CO_2/MEA selectivity.

Considering the evident effect of selectivity on prevention of amine emmision, the selectivity of AF2400/XT-RGO is too low, only offering a reduction of amine emission of approximately 5%. The AF2400/ZIF-8 membrane has a very satisfying CO_2/DEEA selectivity, whereas the CO_2/MAPA selectivity is rather low. However, AF2400/ZIF-8 proved to behave unstable in the membrane contactor considering the CO_2 permeability development with temperature, and it needs to be investigated further if the membrane is feasible at all in membrane contactors.

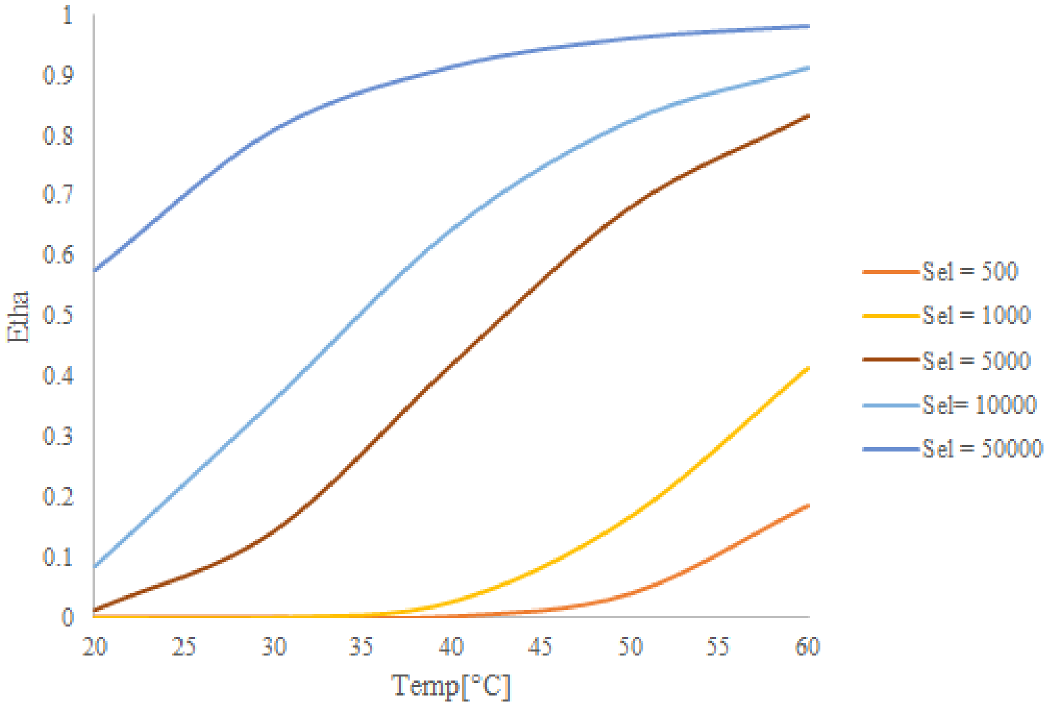

Figure 5.2: Effect of temperature and α_{CO_2} on η. Each line in the plot represents one value of selectivity, α_{CO_2}, shown to the right.

Figure 5.3 shows the effect of weight percent MEA in liquid phase, wMEA and membrane selectivity on η. It shows that increased MEA concentrations in the liquid phase increases the prevention of MEA emissions. This is because an increase in wMEA increase pMEA and thereby η. However, different values of wMEA react differently on η to increased selectivity. The higher weight fraction of MEA, the steeper increase in η against selectivity.

The results indicate that membrane contactors allow a higher MEA liquid concentration compared to conventional CO_2 absorption.

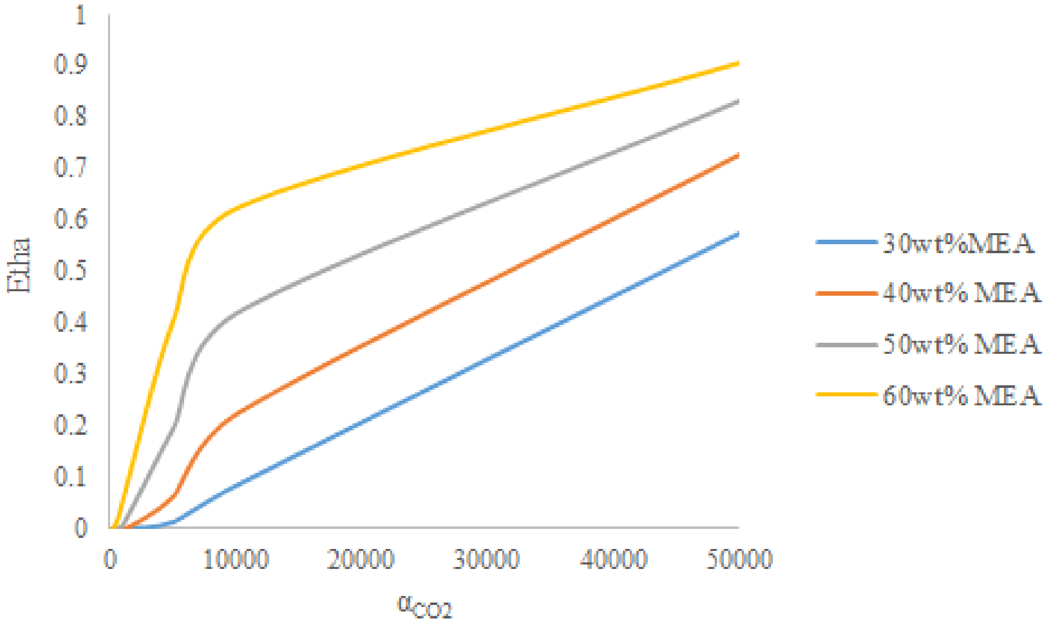

Figure 5.3: Effect of selectivity and wt% MEA in liquid feed on prevention of MEA emission, η.

In Figure 5.4 the effect of general amine volatility and membrane selectivity on prevention of amine emission is shown. The absorbent in this case is hypothetical, with VLE data for MEA but with different levels of volatility.

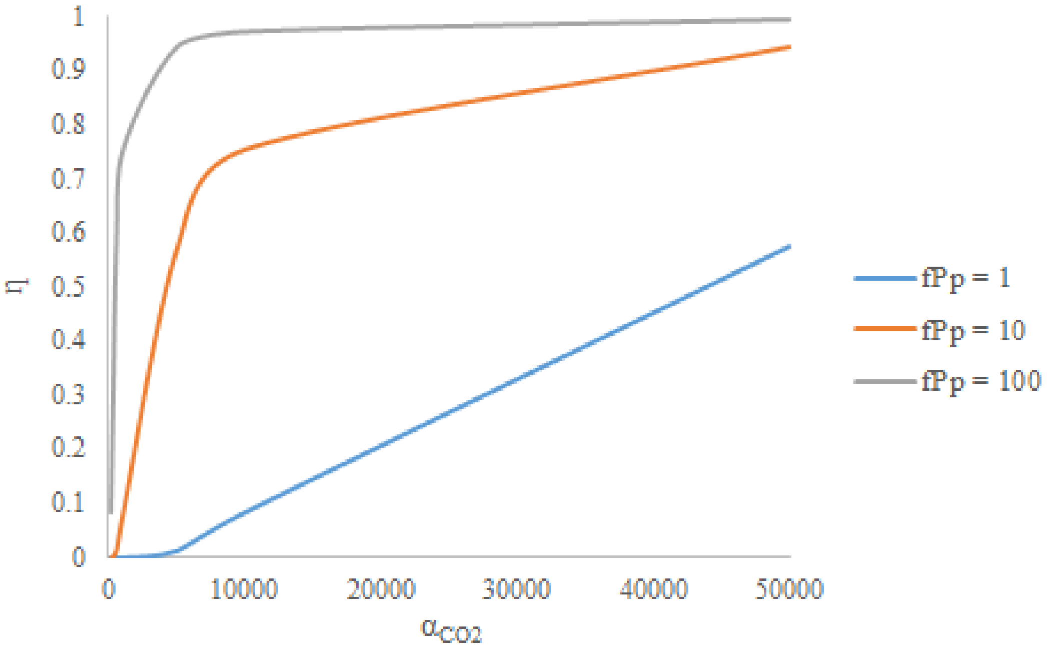

Figure 5.4: Prevention of amine emission η vs selectivity, α_{CO_2} for selected amine volatilites fPp.

It is logical that the advantage of membrane contactors becomes more apparent compared to conventional absorption when volatility is higher. This is due to the fact that the higher volatility, the higher amount of absorbents will evaporate and be released together with the gas stream purified from CO_2. The lower permeability of absorbents through the membrane, the higher the advantage of utilizing membrane contactors. In Section 2.4.3 it was stated that 3D3M has a higher volatility compared to MEA. Together with the result in Figure 5.4 this result supports using 3D3M in membrane contactor setups, as 3D3M has a lower regeneration energy requirement compared to MEA and can thus contribute to a lower energy consumption and thereby operating cost.

With that being said, the CO_2/3D3M selectivity in case of AF200/XT-RGO and AF2400/ZIF-8 did not contribute to a high decrease in amine emmision. The model has yet to include VLE data for 3D3M, which might change the conclusion.

6 Conclusion

The membranes synthesized in this thesis were nanocomposite membranes with AF2400 in polymeric phase, and XT-RGO and ZIF-8 as nanofillers. The ZIF-8 nanocomposite membrane proved to be difficult to homogenize at nanoscale, where both sieve-in-cage structure between ZIF-8 and polymer phase and clustering of ZIF-8 particles was observed. Other high CO_2 permeable membranes were tested for compatibility with the 3rd generation absorbents, but only AF2400 proved to be stable with the solvents.

The amine permeability through the nanocomposite membranes proved to be lower compared to the pure AF2400 membrane, indicating that addition of ZIF-8 and XT-RGO serve to reduce the emission of amines in membrane contactor absorption, which was the aim to prove in this thesis. The quantified reduction however, was different in three membranes tested, where XT-RGO most efficiently reduced MEA permeability, and similarly ZIF-8 reduced 3D3M most efficiently.

According to simulations performed on a simple membrane contactor model, it was found that the CO_2 permeability plays an important role on the feasibility of the membrane contactor, as it affects the amount of membrane modules.

The CO_2 permeability was studied at different levels of relative humidity, where AF2400/ZIF-8 had higher permeability compared to AF2400/XT-RGO. However, the CO_2 permeability of AF2400/XT-RGO was higher in the membrane contactor compared to AF2400/ZIF-8 except at the highest temperature tested, 60°C. The CO_2 permeability of AF2400/ZIF-8 in the membrane contactor proved to be unstable with changes in temperature, meaning that based on the experiments performed in this thesis, AF2400/XT-RGO is the most feasible membrane to use in membrane contactors.

It was shown in the simple membrane contactor model that the CO_2/amine selectivity together with temperature affects the prevention of amine emissions compared to conventional absorption. AF2400/ZIF-8 had a total higher selectivity of 3D3M compared to AF2400/XT-RGO based on mixed gas experiments, but the higher selectivity was less pronounced in the membrane contactor due to a drastic reduction in CO_2 permeability in the membrane contactor. Overall, AF2400/XT-RGO had higher CO_2/amine selectivity compared to the pure AF2400 membrane in case of MEA and MAPA, which confirms that the amine permeability is decreased to a larger extent than the CO_2 permeability in XT-RGO compared to pure AF2400.

Manual dip coating for making membrane modules with pure AF2400 and polypropylene was difficult in case of high polymer concentrations and thin fibers. However, it is shown that the thickness increases linearly with the concentration of polymer, and that dipping twice leads to a thicker membrane layer compared to dipping once.

7 Further research

In order to obtain homogeneous AF2400/ZIF-8 membranes with perfect polymer/nanoparticle interactions, other methods of membrane preparation should be tested. For example, ultrasonication can be optimized or substituted with another technique, such as particle modification of the nanoparticle in order to increase the affinity.

Both AF2400/ZIF-8 and AF2400/XT-RGO should be studied further in the membrane contactor. The temperature area of where the CO_2 permeability starts to increase in the AF2400/ZIF-8 membrane is of specific interest. Also, thinner membranes supported by a supportive layer can be applied in the contactor in order to see if it the performance is better at lower membrane thickness.

It is also interesting to investigate the actual loss of amines in a membrane contactor. It should be investigated if the CO_2/amine selectivity becomes more attractive when the loss of volatility on CO_2 saturated amines are taken into account.

Also, the chemical interactions of nanoparticles and CO_2 absorbents can be studied further in order to understand if the compatibility between the two might affect the performance of the nanocomposite membrane in a membrane contactor. It may also be an option to study other nanofillers or ZIF-8 and XT-RGO at other concentrations.

A model that contains VLE data for 3D3M should be developed and studied in order to see if the properties of 3D3M makes the combination of 3D3M and AF2400/XT-RGO or AF2400/ZIF-8 more attractive in membrane contactors.

References

Aaron, D. and Tsouris, C. (2005). Separation of co2 from flue gas: a review. *Separation Science and Technology*, 40(1-3):321–348.

Adams, M. (2010). Ammonia (NH_3) emissions. `https://www.eea.europa.eu/data-and-maps/indicators/eea-32-ammonia-nh3-emissions-1`. Accessed: 2017-05-04.

Ansaloni, L. (2016). Organic-inorganic hybrid membranes [powerpoint slides]. `https://ntnu.itslearning.com/ContentArea/ContentArea.aspx?LocationID=61342&LocationType=1`.

Ansaloni, L., Arif, A., Ciftja, A. F., Knuutila, H. K., and Deng, L. (2016). Development of membrane contactors using phase change solvents for co2 capture: Material compatibility study. *Industrial & Engineering Chemistry Research*.

Ansaloni, L., Knuutila, H. K., and Deng, L. (2017a). Development of membrane contactors using volatile amine-based absorbents for CO_2 capture: amine permeation through the membrane. *Journal of Membrane Science*.

Ansaloni, L., Rennemo, R., Knuutila, H. K., and Deng, L. (2017b). Development of membrane contactors using volatile amine-based absorbents for co 2 capture: amine permeation through the membrane. *Journal of Membrane Science*.

AZOnano (2017). Reduced graphene oxide: Properties, applications and production methods. `http://www.azonano.com/article.aspx?ArticleID=4041`. Accessed: 2017-05-04.

Baker, R. W. (2002). Future directions of membrane gas separation technology. *Industrial & Engineering Chemistry Research*, 41(6):1393–1411.

Budd, P. M. and McKeown, N. B. (2010). Highly permeable polymers for gas separation membranes. *Polymer Chemistry*, 1(1):63–68.

Chung, T.-S., Jiang, L. Y., Li, Y., and Kulprathipanja, S. (2007). Mixed matrix membranes (mmms) comprising organic polymers with dispersed inorganic fillers for gas separation. *Progress in Polymer Science*, 32(4):483–507.

Ciftja, A. F., Hartono, A., and Svendsen, H. F. (2013). Experimental study on phase change solvents in co 2 capture by nmr spectroscopy. *Chemical Engineering Science*, 102:378–386.

Cong, H., Radosz, M., Towler, B. F., and Shen, Y. (2007). Polymer–inorganic nanocomposite membranes for gas separation. *Separation and Purification Technology*, 55(3):281–291.

D'Alessandro, D. M., Smit, B., and Long, J. R. (2010). Carbon dioxide capture: prospects for new materials. *Angewandte Chemie International Edition*, 49(35):6058–6082.

Deng, L. (2016a). Membrane contactors [powerpoint slides]. Itslearning.

Deng, L. (2016b). Membrane module and process design, chapter 8 [powerpoint slides]. Itslearning.

FC, T. C. C. (2016). Teflon af, amorphous fluoroplastic resins. `https://www.chemours.com/Teflon_Industrial/en_US/assets/downloads/teflon-af-processing-and-use.pdf`. Accessed: 2016-12-12.

Feng, X. and Huang, R. Y. (1997). Liquid separation by membrane pervaporation: a review. *Industrial & Engineering Chemistry Research*, 36(4):1048–1066.

Franco, J. A., Kentish, S. E., Perera, J. M., and Stevens, G. W. (2011). Poly (tetrafluoroethylene) sputtered polypropylene membranes for carbon dioxide separation in membrane gas absorption. *Industrial & Engineering Chemistry Research*, 50(7):4011–4020.

Gabelman, A. and Hwang, S.-T. (1999). Hollow fiber membrane contactors. *Journal of Membrane Science*, 159(1):61–106.

Greeves, N. (2016). Zif-8 metal organic framework. `http://www.chemtube3d.com/solidstate/MOF-ZIF8.htm`. Accessed: 2016-11-22.

Hauge, M. (2016). Hybrid af2400 membranes:effect of nanoparticles on co2permeability and co2/n2selectivity.

Huang, L., Zhang, M., Li, C., and Shi, G. (2015). Graphene-based membranes for molecular separation. *The journal of physical chemistry letters*, 6(14):2806–2815.

Kim, I. and Svendsen, H. F. (2007). Heat of absorption of carbon dioxide (co2) in monoethanolamine (mea) and 2-(aminoethyl) ethanolamine (aeea) solutions. *Industrial & engineering chemistry research*, 46(17):5803–5809.

Kittel, J., Idem, R., Gelowitz, D., Tontiwachwuthikul, P., Parrain, G., and Bonneau, A. (2009). Corrosion in mea units for co2 capture: pilot plant studies. *Energy Procedia*, 1(1):791–797.

Knuutila, H. and Svendsen, H. (2016). Absorption [powerpoint slides]. Itslearning.

Koros, W. J. (2002). Gas separation membranes: needs for combined materials science and processing approaches. In *Macromolecular symposia*, volume 188, pages 13–22. Wiley Online Library.

Li, J.-L. and Chen, B.-H. (2005). Review of co 2 absorption using chemical solvents in hollow fiber membrane contactors. *Separation and Purification Technology*, 41(2):109–122.

Liu, G., Jiang, Z., Cao, K., Nair, S., Cheng, X., Zhao, J., Gomaa, H., Wu, H., and Pan, F. (2017). Pervaporation performance comparison of hybrid membranes filled with two-dimensional zif-l nanosheets and zero-dimensional zif-8 nanoparticles. *Journal of Membrane Science*, 523:185–196.

Los, J., Zakharchenko, K., Katsnelson, M., and Fasolino, A. (2015). Melting temperature of graphene. *Physical Review B*, 91(4):045415.

Low, B. T., Zhao, L., Merkel, T. C., Weber, M., and Stolten, D. (2013). A parametric study of the impact of membrane materials and process operating conditions on carbon capture from humidified flue gas. *Journal of membrane science*, 431:139–155.

Low, Z.-X., Razmjou, A., Wang, K., Gray, S., Duke, M., and Wang, H. (2014). Effect of addition of two-dimensional zif-l nanoflakes on the properties of polyethersulfone ultrafiltration membrane. *Journal of Membrane Science*, 460:9–17.

Lowry, J. H., Mendlowitz, J. S., et al. (1992). Optical characteristics of teflon af fluoroplastic materials. *Optical Engineering*, 31(9):1982–1985.

McCarthy, M. C., Varela-Guerrero, V., Barnett, G. V., and Jeong, H.-K. (2010). Synthesis of zeolitic imidazolate framework films and membranes with controlled microstructures. *Langmuir*, 26(18):14636–14641.

Mertens, J., Lepaumier, H., Desagher, D., and Thielens, M.-L. (2013). Understanding ethanolamine (mea) and ammonia emissions from amine based post combustion carbon capture: Lessons learned from field tests. *International Journal of Greenhouse Gas Control*, 13:72–77.

Nemser, S. M. and Roman, I. C. (1991). Perfluorodioxole membranes. US Patent 5,051,114.

Nguyen, P., Lasseuguette, E., Medina-Gonzalez, Y., Remigy, J., Roizard, D., and Favre, E. (2011). A dense membrane contactor for intensified CO_2 gas/liquid absorption in post-combustion capture. *Journal of membrane science*, 377(1):261–272.

Nguyen, T., Hilliard, M., and Rochelle, G. T. (2010). Amine volatility in co 2 capture. *International Journal of Greenhouse Gas Control*, 4(5):707–715.

Osilla (2017). Reduced graphene oxide. `https://www.ossila.com/products/reduced-graphene-oxide`. Accessed: 2017-05-04.

Pandey, P. and Chauhan, R. (2001). Membranes for gas separation. *Progress in Polymer Science*, 26(6):853–893.

Pinnau, I. and Toy, L. G. (1996). Gas and vapor transport properties of amorphous perfluorinated copolymer membranes based on 2, 2-bistrifluoromethyl-4, 5-difluoro-1, 3-dioxole/tetrafluoroethylene. *Journal of Membrane Science*, 109(1):125–133.

Robeson, L. M. (2008). The upper bound revisited. *Journal of Membrane Science*, 320(1):390–400.

Rochelle, G. T. (2009). Amine scrubbing for co2 capture. *Science*, 325(5948):1652–1654.

Saeed, M. and Deng, L. (2016). Post-combustion co 2 membrane absorption promoted by mimic enzyme. *Journal of Membrane Science*, 499:36–46.

Sigma-Aldrich (2017). Reduced graphene oxide. `http://www.sigmaaldrich.com/catalog/product/aldrich/777684?lang=en&region=NO`. Accessed: 2017-05-05.

Thallapally, P. K., Tian, J., Radha Kishan, M., Fernandez, C. A., Dalgarno, S. J., McGrail, P. B., Warren, J. E., and Atwood, J. L. (2008). Flexible (breathing) interpenetrated metal- organic frameworks for co2 separation applications. *Journal of the American Chemical Society*, 130(50):16842–16843.

Tiwari, R. R., Smith, Z. P., Lin, H., Freeman, B., and Paul, D. (2015). Gas permeation in thin films of “high free-volume” glassy perfluoropolymers: Part ii. CO_2 plasticization and sorption. *Polymer*, 61:1–14.

Tokarev, A., Friess, K., Machkova, J., Šipek, M., and Yampolskii, Y. (2006). Sorption and diffusion of organic vapors in amorphous teflon af2400. *Journal of Polymer Science Part B: Polymer Physics*, 44(5):832–844.

Zhang, K., Lively, R. P., Zhang, C., Chance, R. R., Koros, W. J., Sholl, D. S., and Nair, S. (2013). Exploring the framework hydrophobicity and flexibility of zif-8: from biofuel recovery to hydrocarbon separations. *The Journal of Physical Chemistry Letters*, 4(21):3618–3622.

Zhao, S., Feron, P. H., Deng, L., Favre, E., Chabanon, E., Yan, S., Hou, J., Chen, V., and Qi, H. (2016). Status and progress of membrane contactors in post-combustion carbon capture: A state-of-the-art review of new developments. *Journal of Membrane Science*, 511:180–206.

A Titration error

The measurement of permeate from MEA tests on AF2400 + ZIF-8 membranes gave results in LabX, while for the permeate test from AF2400 + XT-RGO the results were ”not a number” (NaN). The titration curve of one of the permeate samples of AF2400 + XT-RGO is shown in Figure A.1 and a titration curve of a measurable concentration of MEA is shown in Figure A.2. The abrupt decrease in pH with addition of acid is evident in the measurable MEA sample, while this is not observed in the permeate sample from AF2400 + XT-RGO. This implies that the sample is below the measurable value of the titrator (0.01 mol/kg), which led to the decision of studying the permeate samples form AF2400 + XT-RGO in ion chromatography instead of titration.

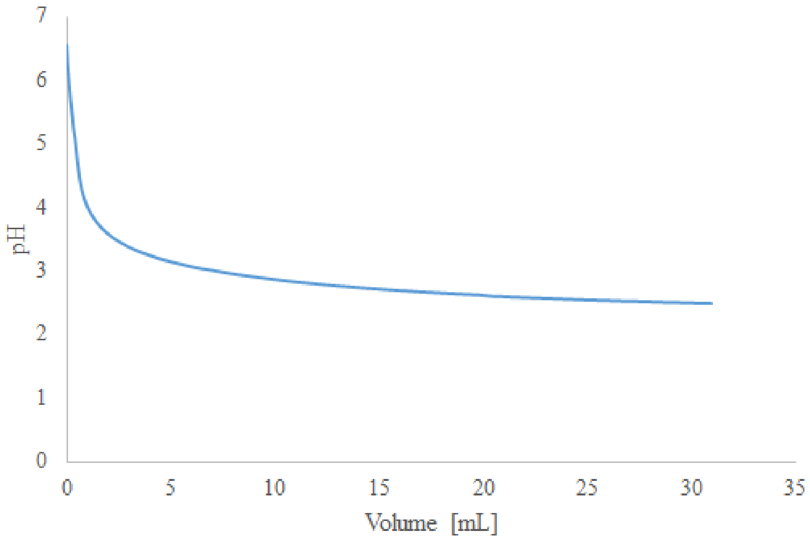

Figure A.1: Titration of a not measurable concentration of MEA in LabX.

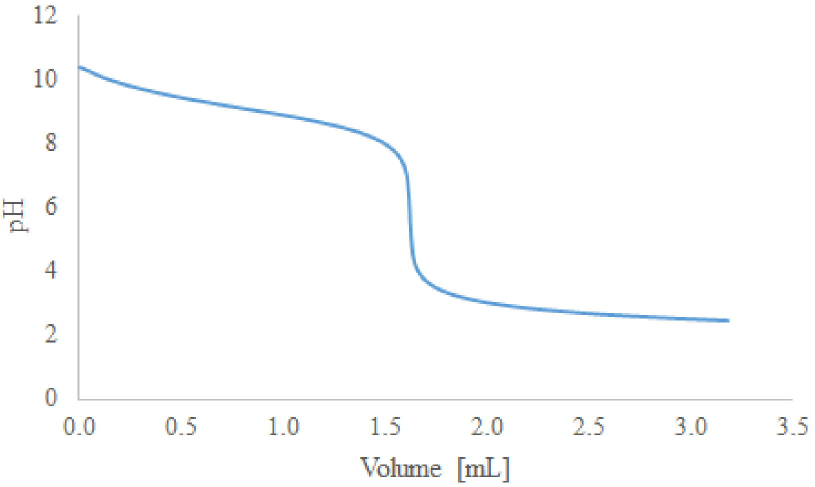

Figure A.2: Titration of a measurable concentration of MEA in LabX.

B Membrane preparation

In Table B.1 the concentration and thickness of the membranes tested later in this section is given.

Table B.1: Concentration and thickness of the membranes tested in this section.

Membrane	Conc.%	Application	Thickness [μm]	STD [μm]
AF2400/XT-RGO	2.5	Mixed gas	23.2	3.51
AF2400/XT-RGO	2.5	Pervaporation	12.6	2.27
AF2400/XT-RGO	2.2	Membrane contactor	6.3	1.64
AF2400/ZIF-8	3.1	Mixed gas	41.5	7.35
AF2400/ZIF-8	3.3	Pervaporation	7.6	2.27
AF2400/ZIF-8	3.3	Membrane contactor	7.3	1.96

The aim was to obtain the same concentration for the nanocomposite membranes and the same thickness for membranes tested in the same application, but this proved to be difficult. In case of thickness, this implies that all values of permeability are given in Barrer which is an intensive parameter independent of thickness and not as permeance which depends on the thickness.

Images of the membranes are presented in Figure B.1. The AF2400/XT-RGO and AF2400/ZIF-8 membranes are samples from the membranes that were tested in the gas permeation setup, while the pure AF2400 membrane is from the project thesis last fall.

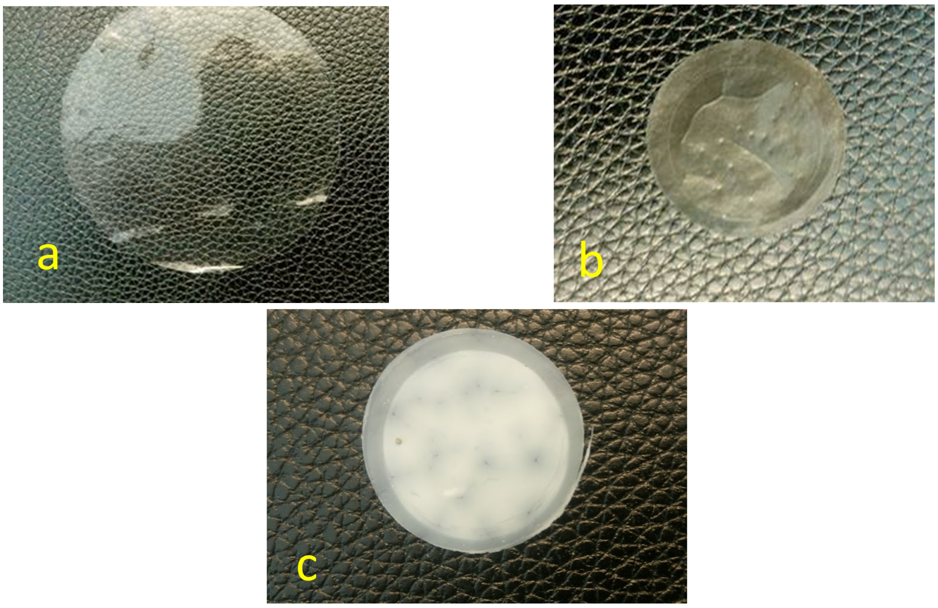

Figure B.1: Membrane photos of (a) Pure AF2400 (b) AF2400/XT-RGO (c) AF2400/ZIF-8.

C Selectivity calculation

In order to calculate the membrane selectivity of CO_2 and absorbents, there had to be made some estimations. The pervaporation test was run at 50 °C while the CO_2 permeability tests were run at 25, 40 and 60 °C.

First, the relative humidity, RH corresponding to the pervaporation test had to be calculated. This was found from Equation C.1:

$$RH \approx \frac{P^*_{\mathrm{H_{20}}}(i,T) \cdot x_{\mathrm{H_2O}} \cdot \gamma_{\mathrm{H_2O}}}{P^*_{\mathrm{H_{20}}}(i,T)} \tag{C.1}$$

Where $P^*_{\mathrm{H_{20}}}(i,T)$ is partial pressure of water in absorbent i at temperature T and $P^*_{\mathrm{H_{20}}}(T)$ is partial pressure of water at temperature T. These two terms cancel, and Equation C.2 is left:

$$RH \approx x_{\mathrm{H_2O}} \cdot \gamma_{\mathrm{H_2O}} \tag{C.2}$$

Where $x_{\mathrm{H_2O}}$ is molfraction of water in absorbent i, and $\gamma_{\mathrm{H_2O}}$ is activity coefficient of water at temperature T. The molfraction of water was found from the mol/L of absorbents (3M DEEA + 3M MAPA and 5M MEA). The activity coefficients of water was found from Ansaloni et al. (2017b). In Table C.1 the activity coefficients, molfractions and calculated relative humidities are shown.

Table C.1: Values for molar fraction ($X_{\mathrm{H_2O}}$) and activity coefficient ($\gamma_{\mathrm{H_2O}}$) of water in 3D3M and 5 M MEA for different temperatures, resulting in the relative humidity, RH for a pervaporation system at the given conditions.

Absorbent	Temp. [°C]	$X_{\mathrm{H_2O}}$	$\gamma_{\mathrm{H_2O}}$	RH [%]
3D3M	25	0.728	0.956	69.9
3D3M	40	0.728	0.989	72.0
3D3M	60	0.728	1.018	74.1
5M MEA	25	0.889	0.991	88.1
5M MEA	40	0.889	0.990	88.0
5M MEA	60	0.889	0.990	88.0

The values of relative humidity were later interpolated from a polynominal regression of the datasets in Figure 4.9 in Section 4.3 in order to find the CO_2 permeability at the given relative humidity and temperature. The three resulting values of permeability are plotted together with temperature in figures C.1 - C.4:

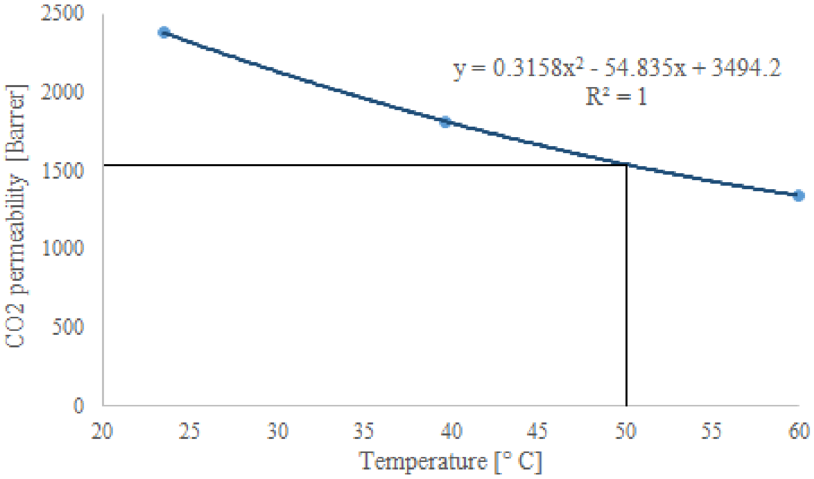

Figure C.1: Interpolation of CO_2 permeability through AF2400/XT-RGO at 50 °C for 3D3M.

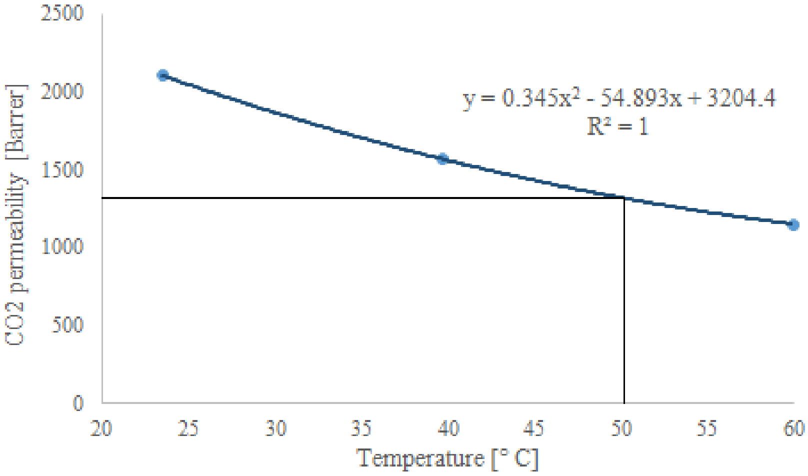

Figure C.2: Interpolation of CO_2 permeability through AF2400/XT-RGO at 50 °C for MEA.

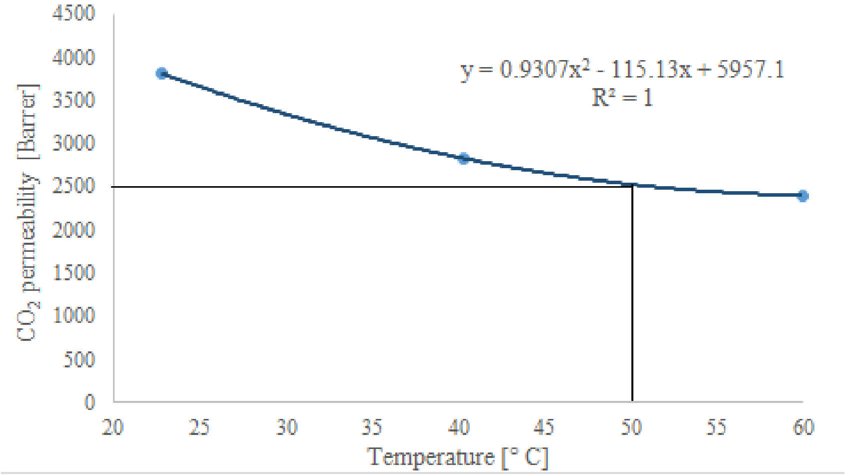

Figure C.3: Interpolation of CO_2 permeability through AF2400/ZIF-8 at 50 °C for 3D3M.

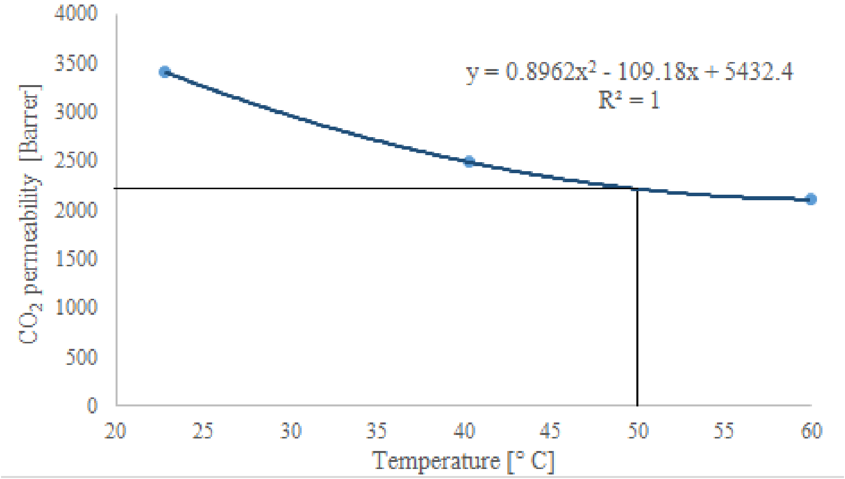

Figure C.4: Interpolation of CO_2 permeability through AF2400/ZIF-8 at 50 °C for MEA.

The interpolated values of CO_2 permeability at 50 °C at the relative humidity corresponding to pervaporation experiments on MEA and 3D3M are given in Table C.2. The data for pure AF2400 was from Ansaloni et al. (2017b).

Table C.2: Interpolated CO_2 permeabilities from figures C.1 to C.4 and Ansaloni et al. (2017b).

Membrane	Absorbent	Temp. [°C]	CO_2 perm. [Barrer]
AF2400/XT-RGO	3D3M	50	1549
AF2400/XT-RGO	5M MEA	50	1322
AF2400/ZIF-8	3D3M	50	2527
AF2400/ZIF-8	5M MEA	50	2214
AF2400	3D3M	50	2444
AF2400	MEA	50	2358

The rest of the selectivity calculation follows a method based on equations given by Ansaloni et al. (2017b). Selectivity, is defined in Equation 5.2, and depends on flux which is defined in Equation 2.2. Based on Equation 2.3, it is possible to calculate the flux from permeability. The selectivity can then be shown as Equation C.3

$$\alpha = \frac{\frac{P_{\mathrm{CO}_2} \cdot \Delta p_{CO2}}{l}}{\frac{P_{amine} \cdot \Delta p_{amine}}{l}} \tag{C.3}$$

An ideal membrane is considered with thickness 1 μm, so l terms cancel, and Equation C.4 is left:

$$\alpha = \frac{P_{\mathrm{CO}_2} \cdot \Delta p_{\mathrm{CO}_2}}{P_{amine} \cdot \Delta p_{amine}} \tag{C.4}$$

Now, P_{CO_2} is known from either mixed gas or membrane contactor experiments, and P_{amine} is known from the pervaporation experiment. Δp_i is found from Equation C.5:

$$\Delta p_i = \gamma_i(T, x_i) \cdot P_i(T) \cdot x_i - p_{down} \cdot y_i \tag{C.5}$$

Where $\gamma_i(T, x_i)$ is the activity coefficient at temperature T and molfraction in liquid, x_i, and $P_i(T)$ is the saturation pressure of compound i at temperature T. In case of amines, the p_{down} term can be neglected since it is so small compared to the other term.

The saturation pressure $P_i(T)$ is found from the Antoine Equation C.6 in case of 3D3M:

$$log p_i(T) = A - \frac{B}{C + T} \tag{C.6}$$

And $p_i(T)$ for MEA is found from Antoine equation C.7:

$$ln p_i(T) = A - \frac{B}{C + T} \tag{C.7}$$

Where the parameters A, B and C are given in Table C.3:

Table C.3: Antoine parameters for MEA, MAPA and DEEA (Ansaloni et al., 2017b).

Absorbent	A	B	C
MEA	7.8709	1819.8	194.62
DEEA	13.92	3198	89.9
MAPA	14.86	3530.43	67.82

The values in Table C.3 inserted in Equation C.6 and C.7 and converted to Bar, are given in Table C.4:

Table C.4: Saturation pressure of MEA, MAPA and DEEA at 25°C, 40°C and 60°C.

Absorbent	p(25°C) [Bar]	p(40°C) [Bar]	p(50°C) [Bar]	p(60°C) [Bar]
MEA	$8.80 \cdot 10^{-}4$	$1.50 \cdot 10^{-}3$	$2.5 \cdot 10^{-}3$	$2.75 \cdot 10^{-}3$
MAPA	$3.30 \cdot 10^{-}3$	$2.89 \cdot 10^{-}2$	$1.06 \cdot 10^{-}1$	$3.52 \cdot 10^{-}1$
DEEA	$3.56 \cdot 10^{-}4$	$3.85 \cdot 10^{-}3$	$1.59 \cdot 10^{-}2$	$5.82 \cdot 10^{-}2$

Finally, the calculated Δp_i values are shown in Table C.5. The selectivity can now be found from values in Table C.2 and C.5, Figure 4.11 and Δp_{CO_2} in the mixed gas experiments.

Table C.5: Final Δp_i values for MEA, MAPA and DEEA.

Absorbent	Temp. [°C]	x_i	$gamma_i$	p_i [Bar]	Δp_i [Bar]
MEA	50	0.111	0.38	0.0025	$1.05 \cdot 10^{-}4$
MAPA	50	0.136	0.18	0.106	$2.61 \cdot 10^{-}3$
DEEA	50	0.136	2.49	0.0159	$5.39 \cdot 10^{-}3$

D Morphology of hollow fibers

In Section 4.6 results from membrane layer thickness on tubular fibers are given based on number of dips in coating solution and concentration of solution. In Figure D.1 some SEM images from the thickness study is shown, representing all three sizes of fibers.

All the big fibers studied were perfectly covered by the AF2400 layer with no folds or gaps between layer and fiber, as shown in Figure D.1 (a). For the medium fibers studied, only the fiber dipped twice in 3.5 wt% solution had folds and gaps between the fiber and AF2400 layer, which can be seen in Figure D.1 (b). For the small fibers all fibers experienced low quality coating with both folds and gaps.

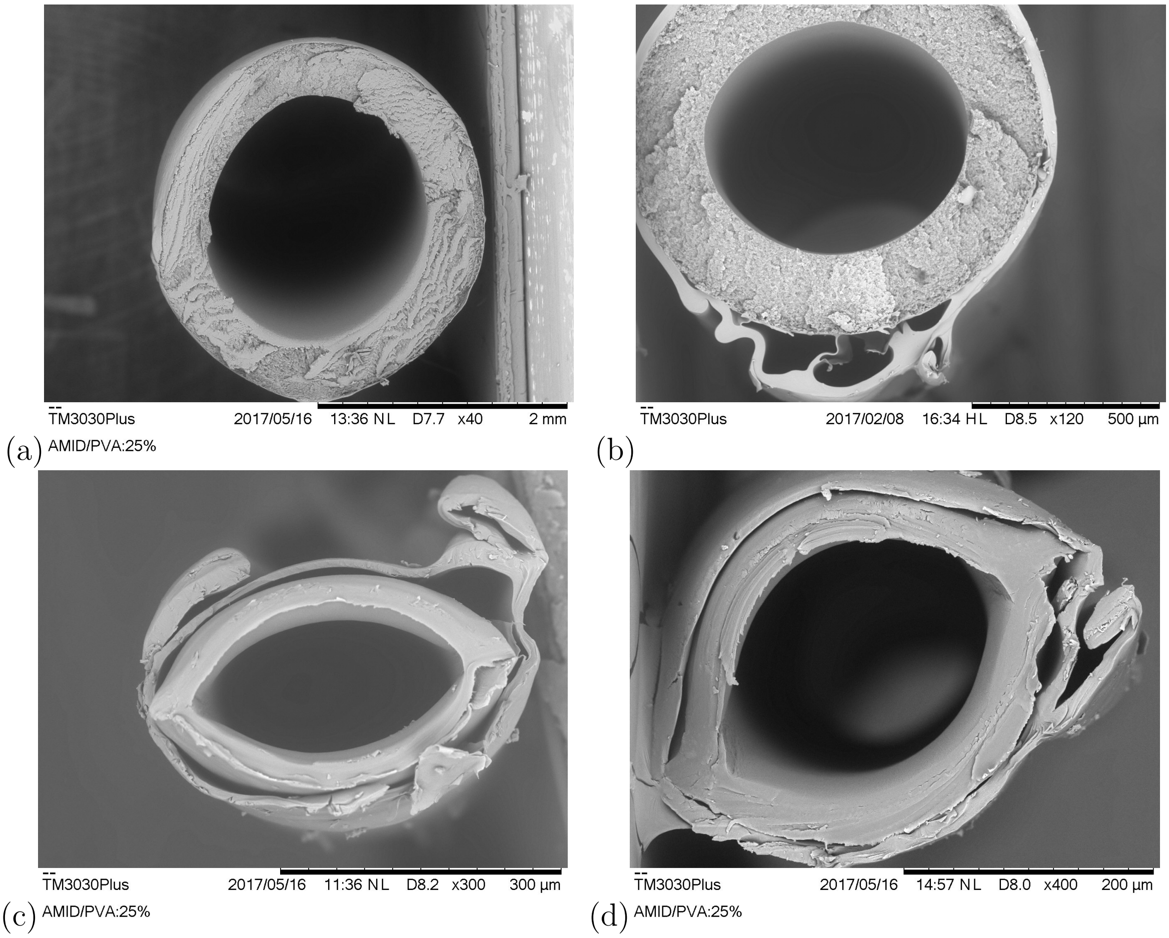
TM3030Plus
2017/05/16 13:36 N L D7.7 x40 2 mm
(a)
AMID/PVA:25%
TM3030Plus
2017/02/08 16:34 H L D8.5 x120 500 µm
(b)
TM3030Plus
2017/05/16 11:36 N L D8.2 x300 300 µm
(c)
AMID/PVA:25%
TM3030Plus
2017/05/16 14:57 N L D8.0 x400 200 µm
(d)
AMID/PVA:25%

Figure D.1: (a) Cross-section SEM image big sized tubular fiber coated in 3.5 wt% AF2400. (b) Cross-section SEM image of medium sized tubular fiber coated in 3.5 wt% AF2400. (c) Cross-section SEM image of small sized tubular fiber coated with 3.5 wt% AF2400. (d) Cross-section SEM image of small sized tubular fiber coated with 2.5 wt% AF2400.

E Sensitivity analysis of simple membrane model

A sensitivity analysis was performed on the simple membrane contactor module in order to see which parameters that affected the amine evaporation and the number of membrane modules/area.

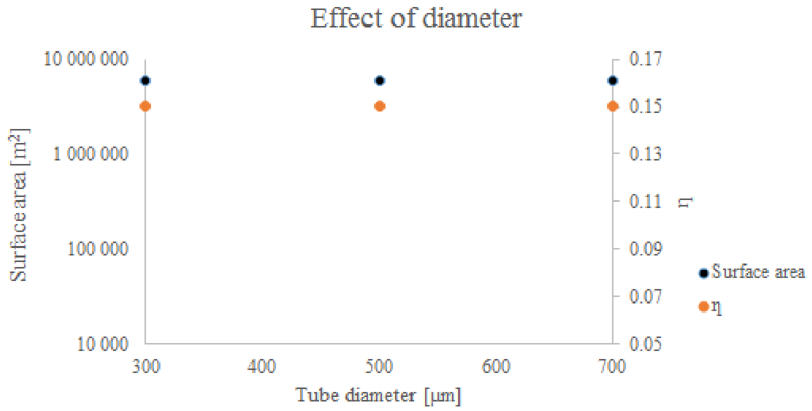

Figure E.1: Effect of tubular diameter on total surface area and prevention of amine emission when all other parameters are held constant.

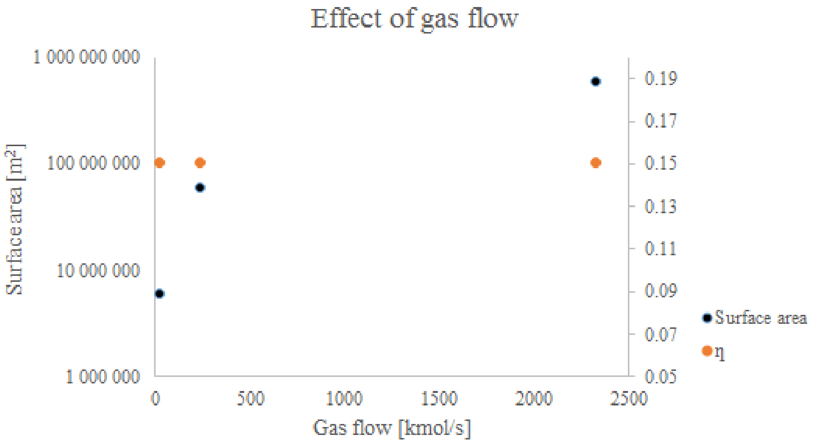

Figure E.2: Effect of gas flow on total surface area and prevention of amine emission when all other parameters are held constant.

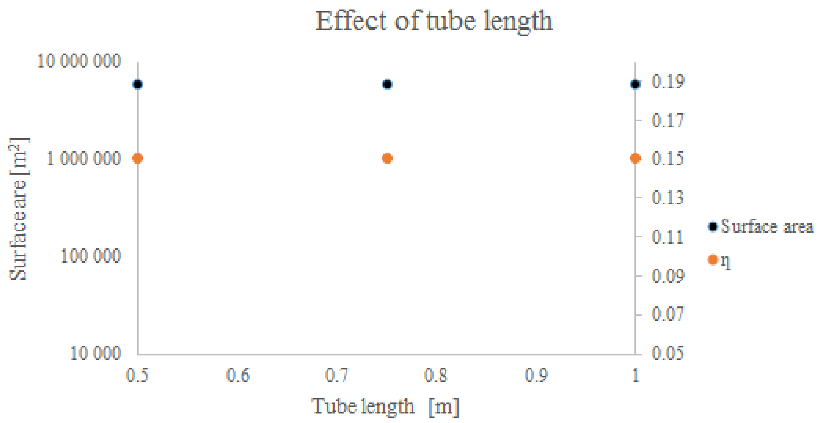

Figure E.3: Effect of tube length on total surface area and prevention of amine emission when all other parameters are held constant.

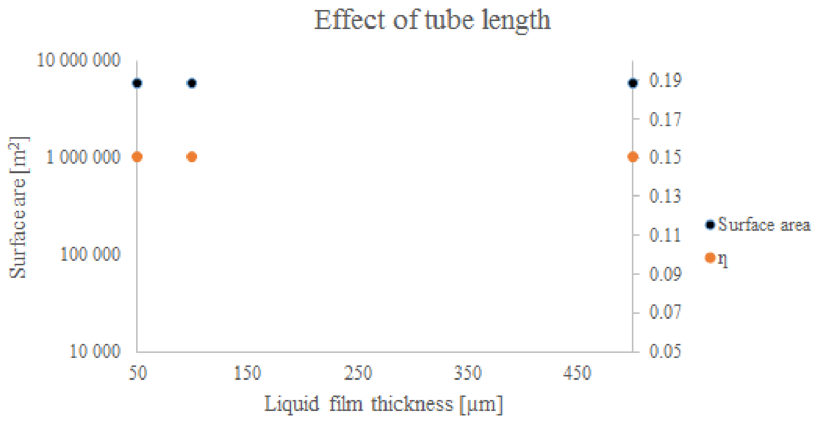

Figure E.4: Effect of tube length on total surface area and prevention of amine emission when all other parameters are held constant.